AUT Journal of Mechanical Engineering

AUT J. Mech. Eng., 1(2) (2017) 191-210
DOI: 10.22060/mej.2017.12329.5314

A Parametric Study on Flutter Analysis of Cantilevered Trapezoidal FG Sandwich Plates

H. Afshari[1], K. Torabi[2*]

[1] Department of Mechanical Engineering, Khomeinishahr Branch, Islamic Azad University, Khomeinishahr/Isfahan, Iran
[2] Faculty of Mechanical Engineering, University of Isfahan, Isfahan, Iran

ABSTRACT: In this paper, supersonic flutter analysis of cantilevered trapezoidal plates composed of two functionally graded face sheets and an isotropic homogeneous core is presented. Using Hamilton's principle, the set of governing equations and external boundary conditions are derived. A transformation of coordinates is used to convert the governing equations and boundary conditions from the original coordinates into the new dimensionless computational ones. Generalized differential quadrature method (GDQM) is employed as a numerical method and critical aerodynamic pressure and flutter frequencies are derived. Convergence, versatility, and accuracy of the presented solution are confirmed using numerical and experimental results presented by other authors. The effect of power-law index, thickness of the core, total thickness of the plate, aspect ratio and angles of the plate on the flutter boundaries are investigated. It is concluded that any attempt to increase the critical aerodynamic pressure leads to a decrease in lift force or rise in total weight of the plate.

Review History:
Received: 8 January 2017
Revised: 10 March 2017
Accepted: 7 May 2017
Available Online: 11 September 2017

Keywords:
Aeroelasticity
Flutter
Trapezoidal plate
Sandwich plate

1- Introduction

There are extensive usages of trapezoidal plates in many structures, especially in aircrafts [1, 2]. As flight velocity of an aircraft increases, the aeroelastic self-excited oscillation of the wing or tail fin will occur which is known as the aeroelastic flutter. Flutter is a critical dynamic problem which is very dangerous to the aircraft safety; therefore, numerous researchers have studied the flutter characteristics of various structures. As the complexities appeared in the governing equations, many authors used numerical approaches, e.g. Finite element method (FEM) and Galerkin method, and presented approximate results for flutter characteristics of structures.

Based on the classical plate theory for structural modeling and piston theory for aerodynamic pressure, Srinivasan and Babu [3] presented FEM model for flutter analysis of isotropic quadrilateral plates. They derived both critical dynamic pressure and flutter frequency for various boundary conditions. Chowdary et al. [4] used a shear deformable element to investigate the supersonic flutter of composite skew plates. They investigated the effect of skew angle on the critical dynamic pressure for different boundary conditions and fiber orientation. Using FEM, Singha and Ganapathi [5] considered both shear deformation and rotational inertia and presented a parametric study on supersonic flutter behavior of laminated composite skew plates. They investigated the effect of different parameters such as skew angle, fiber orientation, and boundary conditions on the critical aerodynamic pressure. Prakash and Ganapathi [6] used FEM and studied the influence of thermal environment on the supersonic flutter behavior of flat panels made of functionally graded materials. The aerodynamic force was evaluated by considering the first-order high Mach number approximation to linear potential flow theory. Using isoparametric finite element formulation, Singha and Mandal [7] investigated supersonic panel flutter behavior of laminated composite plates and cylindrical panels. They studied the effects of curvature, laminate stacking sequence, air flow direction and boundary condition on the supersonic flutter characteristics. Using FEM and quasi-steady aerodynamic theory, the effect of variable fiber spacing on the supersonic flutter of rectangular composite plates has been investigated by Kuo [8]. He showed that flutter boundaries may be increased or decreased due to variable fiber spacing. Meijer and Dala [9] used a finite element structural model based on Mindlin-Reissner theory for the plate and local piston theory for aerodynamic pressure in supersonic flow and developed a zeroth-order flutter prediction for cantilevered plates. They validated their method against published experimental data. Based on higher-order structural theory and using QUAD-8 shear flexible shell element, Sankar et al. [10] presented the supersonic flutter characteristics of doubly curved sandwich shell panels with carbon nanotube (CNT) reinforced face sheets. They investigated the influence of the volume fraction of the CNT, core-to-face sheet thickness, the shell thickness and the aspect ratio, radius-to-thickness ratio, and temperature on the flutter boundaries. Using FEM, Cunha-Filho et al. [11] presented a numerical study on the flutter analysis of a three-layer sandwich rectangular plate and investigated the possibility of reducing the effects of the supersonic aeroelastic instability of plates by applying passive constrained viscoelastic layers.

Using Galerkin method, Navazi and Haddadpour [12] studied the nonlinear aeroelastic behavior of homogeneous and

Corresponding author, E–mail: k.torabi@eng.ui.ac.ir

functionally graded two dimensional and three-dimensional flat plates under supersonic airflow. They used the von-Karman nonlinear strains, piston theory and a combination of simple rule of mixtures and the Mori-Tanaka scheme to model the structure, aerodynamic and material, respectively. They showed that under real flight conditions and using coupled model, the aerodynamic heating is very severe and the type of instability is divergent. Vedeneev [13, 14] used Galerkin method and focused on the single mode panel flutter analysis which happens at low supersonic speeds. He presented a comprehensive numerical solution of single-mode flutter [13]. As he used Euler-Bernoulli beam theory, results were applicable to the panels of high aspect ratios. He also investigated the effect of damping on single mode panel flutter of simply supported and clamped panels at low supersonic speeds [14]. He showed that for typical structural, damping levels single-mode flutter is not always avoidable. Moreover, for some conditions damping level necessary to suppress flutter is too high and cannot be achieved by the structure itself. Based on the classical Love's shell theory and the first-order piston theory for aerodynamic loading and using Galerkin method, Haddadpour et al. [15] and Mahmoudkhani et al. [16] considered temperature-dependent properties and studied supersonic aero-thermoelastic analysis of a functionally graded cylindrical and truncated conical shells, respectively. For the cylindrical shell they investigated the effects of power-law index, internal pressure and temperature rise on the flutter boundaries and for the conical one, they predicted the flutter boundaries for different values of semi-vertex cone angles, different temperature distributions, and different volume fraction indices. Using Galerkin method, Kouchakzadeh et al. [17] investigated the problem of nonlinear aeroelasticity of a general laminated composite plate in supersonic air. They hired the classical plate theory along with the von-Karman nonlinear strains for structural modeling and linear piston theory for aerodynamic modeling and studied the effects of in-plane force, static pressure differential, fiber orientation and aerodynamic damping on the nonlinear aeroelastic behavior of the plate and showed that the fiber orientation has a significant effect on dynamic behavior of the plate.

Li and Nartia [18, 19] focused on the optimization of structure to increase the critical aerodynamic pressure; They used a layerwise optimization approach and obtained the optimal fiber orientation angles of the supersonic laminated plate to obtain the maximum critical aerodynamic pressure [18]. They showed that through the optimization process, one can largely raise the critical aerodynamic pressure and significantly improve the stability of supersonic plates. In another work, they presented a multi-objective optimal design of aeroelastic laminated doubly curved shallow shells modeled based on the first-order shear deformation theory [19]. They considered the fiber orientations in the layers of the symmetrically angle-ply shells as the design variable and the maximization of the weighted sum of the critical aerodynamic pressures under different probability density functions of flow orientations as the design objective.

Recently, Torabi and Afshari [20] have employed particle swarm optimization (PSO) and found the optimum geometric shape of a cantilevered trapezoidal homogeneous plate with a non-uniform thickness which has the maximum value of the critical aerodynamic pressure. They did not investigate the effect of geometrical parameters of the plates on the flutter boundaries and focused on the optimization procedure. In this paper, authors expand this work and present a parametric study on the flutter analysis of a cantilevered trapezoidal sandwich plate made of functionally graded materials. The plate is composed of two functionally graded face sheets and an isotropic homogeneous core. The set of governing equations are obtained and are solved numerically using GDQM and the effect of power-law index, thickness of the core, total thickness of the plate, aspect ratio and angles of the plate on the flutter boundaries are investigated. It is worth mentioning that in spite of having wide industrial applications, the cantilevered plate problem is one of the most difficult boundary conditions to be solved. In fact, it is because of the complexities which appear at three free edges.

2- Governing Equations

As depicted in Fig. 1, a cantilevered trapezoidal plate clamped at y=0 and free at other edges is considered. It is assumed that the plate is exposed to a compressible supersonic flow of density ρ_∞ and velocity U_∞ in x direction.

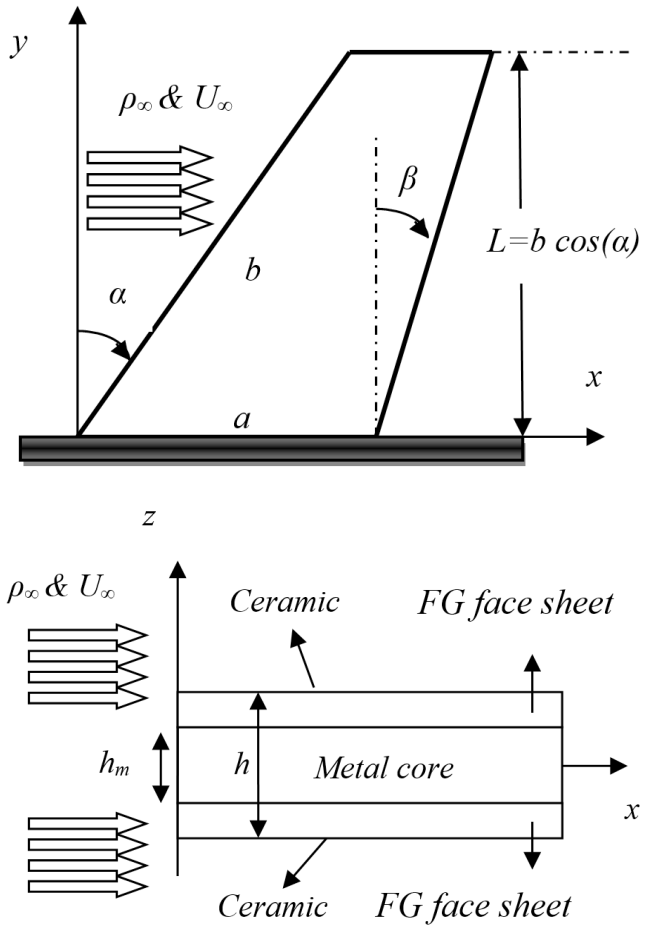

Fig. 1. A trapezoidal functionally graded sandwich plate in a compressible supersonic flow.

The plate is considered to be composed of a homogeneous metal core and two FG face sheets which their properties vary from interior ceramic-rich layers to interior metal-rich ones according to a power law function. Thus, volume fraction of the metal (V_m) and ceramic (V_c) can be considered as

$$V_m(z)=\begin{cases}\left(\dfrac{h+2z}{h-h_m}\right)^q & -\dfrac{h}{2}\le z\le -\dfrac{h_m}{2}\\ 1 & -\dfrac{h_m}{2}\le z\le \dfrac{h_m}{2}\\ \left(\dfrac{h-2z}{h-h_m}\right)^q & \dfrac{h_m}{2}\le z\le \dfrac{h}{2}\end{cases} \qquad (1)$$
$$V_c(z)=1-V_m(z)$$

where q is the power law index. Any properties of the plate (P) can be presented as

$$P(z)=P_c+(P_m-P_c)V_m \qquad (2)$$

in which subscripts "c" and "m" indicate corresponding properties in ceramic and metal, respectively. It should be noticed that usually in FG-structures Poisson's ratio (υ) is considered to be constant.

By introducing dimensionless spatial parameter as $Z=2z/h$, Eq. (1) can be written as

$$V_m(Z)=\begin{cases}\left(\dfrac{1+Z}{1-\kappa}\right)^q & -1\le Z\le -\kappa\\ 1 & -\kappa\le Z\le \kappa\\ \left(\dfrac{1-Z}{1-\kappa}\right)^q & \kappa\le Z\le 1\end{cases} \qquad (3)$$
$$V_c(Z)=1-V_m(Z)$$

where $\kappa=h_m/h$ is the dimensionless thickness of the core.

Unless mentioned otherwise, in this paper numerical results are presented for a functionally graded sandwich plate composed of aluminum (Al) as metal and alumina (Al_2O_3) as ceramic. Mechanical properties of these materials are given in Table 1.

Table 1. Mechanical properties of materials [21].

Material	Properties		
	E (GPa)	ρ (kg/m^3)	υ
Aluminum (Al)	70	2702	0.3
Alumina (Al_2O_3)	380	3800	0.3

For κ=0.5 and various values of power-law index, the variation of the volume fraction of ceramic is illustrated in Fig. 2. This figure indicates that as the value of the q increases or value of κ decreases, the volume fraction of the ceramic grows. Thus, according to Table 1, both stiffness and mass of the plate increase as the value of the q increases or value of κ decreases.

According to the Reissner-Mindlin plate theory, the displacement field is considered as follows [22]:

$$\begin{aligned}u^z(x,y,z)&=u(x,y)+z\psi_x(x,y),\\ v^z(x,y,z)&=v(x,y)+z\psi_y(x,y),\\ w^z(x,y,z)&=w(x,y),\end{aligned} \qquad (4)$$

where u^z, v^z and w^z show the components of displacement along x, y and z directions, respectively; u, v and w indicate corresponding components of displacement on the middle surface (z=0) and ψ_x and ψ_y are rotations about y and x axes, respectively.

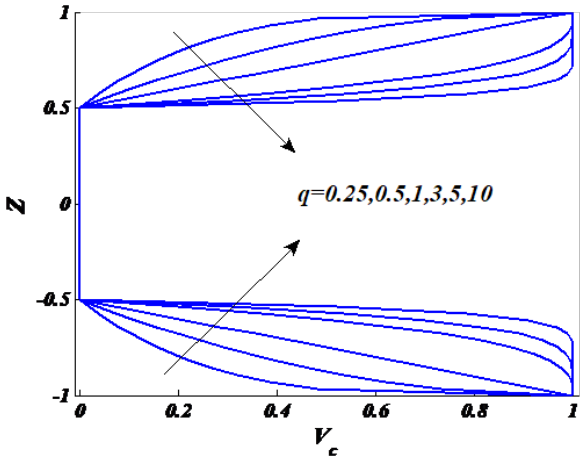

Fig. 2. Variation of the volume fraction of ceramic through the thickness.

For symmetric sandwich plates there is no coupling between in-plane and transverse vibrations; consequently, by neglecting in-plane deformations of the plate at the middle surface, Eq. (4) can be written as

$$\begin{aligned}u^z(x,y,z)&=z\psi_x(x,y),\\ v^z(x,y,z)&=z\psi_y(x,y),\\ w^z(x,y,z)&=w(x,y).\end{aligned} \qquad (5)$$

Components of strain in plate can be stated as [2]

$$\begin{aligned}\varepsilon_x&=z\frac{\partial\psi_x}{\partial x}, \quad \gamma_{xy}=z\left(\frac{\partial\psi_x}{\partial y}+\frac{\partial\psi_y}{\partial x}\right),\\ \varepsilon_y&=z\frac{\partial\psi_y}{\partial y}, \qquad \gamma_{xz}=\psi_x+\frac{\partial w}{\partial x},\\ \varepsilon_z&=0, \qquad \gamma_{yz}=\psi_y+\frac{\partial w}{\partial y}.\end{aligned} \qquad (6)$$

Furthermore, by neglecting σ_z in comparison with σ_x and σ_y in Hook's laws, the components of stress can be stated as [2]

$$\begin{aligned}\sigma_x&=\frac{Ez}{1-\upsilon^2}\left(\frac{\partial\psi_x}{\partial x}+\upsilon\frac{\partial\psi_y}{\partial y}\right),\\ \sigma_y&=\frac{Ez}{1-\upsilon^2}\left(\frac{\partial\psi_y}{\partial y}+\upsilon\frac{\partial\psi_x}{\partial x}\right),\\ \sigma_z&=0,\\ \sigma_{xy}&=G_s z\left(\frac{\partial\psi_x}{\partial y}+\frac{\partial\psi_y}{\partial x}\right),\\ \sigma_{xz}&=kG_s\left(\psi_x+\frac{\partial w}{\partial x}\right),\\ \sigma_{yz}&=kG_s\left(\psi_y+\frac{\partial w}{\partial y}\right).\end{aligned} \qquad (7)$$

in which E and G_s are the modulus of elasticity and shear modulus, respectively and k is shear correction factor which is calculated in this paper using the following relation [23]:

$$k=(5+5\upsilon)/(6+5\upsilon). \tag{8}$$

According to Hamilton's principle, considering δ as variation operator, t as time and $[t_1,t_2]$ as the desired time interval, the set of governing equations and boundary conditions can be derived using the following relation:

$$\delta\int_{t_1}^{t_2}(T-U+W_f)dt=0, \tag{9}$$

where T, U and W_f are kinetic energy, strain energy and work done by external forces, respectively. These parameters are calculated as

$$T=\frac{1}{2}\iiint_V \rho\left[\left(\frac{\partial u^z}{\partial t}\right)^2+\left(\frac{\partial v^z}{\partial t}\right)^2+\left(\frac{\partial w^z}{\partial t}\right)^2\right]dV, \tag{10a}$$

$$U=\frac{1}{2}\iiint_V \begin{pmatrix}\sigma_x\varepsilon_x+\sigma_y\varepsilon_y+\sigma_z\varepsilon_z\\+\sigma_{xy}\gamma_{xy}+\sigma_{xz}\gamma_{xz}+\sigma_{yz}\gamma_{yz}\end{pmatrix}dV, \tag{10b}$$

$$W_f=\iint_S f(x,y,t)w(x,y,t)dS, \tag{10c}$$

in which ρ is the density of the material, V is the volume of the plate, S is an area of the plate at the middle surface and f is external force per unit area. By inserting Eqs. (5), (6), (10-a) to (10-c) into Eq. (9), the set of governing equations can be derived as

$$\begin{aligned}&\frac{\partial Q_{xz}}{\partial x}+\frac{\partial Q_{yz}}{\partial y}-I_0\frac{\partial^2 w}{\partial t^2}+f=0,\\&\frac{\partial M_{xx}}{\partial x}+\frac{\partial M_{xy}}{\partial y}-Q_{xz}-I_2\frac{\partial^2\psi_x}{\partial t^2}=0,\\&\frac{\partial M_{yy}}{\partial y}+\frac{\partial M_{xy}}{\partial x}-Q_{yz}-I_2\frac{\partial^2\psi_y}{\partial t^2}=0,\end{aligned} \tag{11}$$

where

$$\begin{aligned}&\begin{Bmatrix}M_{xx}\\M_{yy}\\M_{xy}\end{Bmatrix}=\int_{-\frac{h}{2}}^{\frac{h}{2}} z\begin{Bmatrix}\sigma_x\\\sigma_y\\\sigma_{xy}\end{Bmatrix}dz,\\&\begin{Bmatrix}Q_{xz}\\Q_{yz}\end{Bmatrix}=\int_{-\frac{h}{2}}^{\frac{h}{2}}\begin{Bmatrix}\sigma_{xz}\\\sigma_{yz}\end{Bmatrix}dz,\quad \begin{Bmatrix}I_0\\I_2\end{Bmatrix}=\int_{-\frac{h}{2}}^{\frac{h}{2}}\begin{Bmatrix}1\\z^2\end{Bmatrix}\rho dz.\end{aligned} \tag{12}$$

Using Eqs. (7) and (12), one can write

$$\begin{aligned}&M_{xx}=D\left(\frac{\partial\psi_x}{\partial x}+\upsilon\frac{\partial\psi_y}{\partial y}\right),\\&M_{yy}=D\left(\upsilon\frac{\partial\psi_x}{\partial x}+\frac{\partial\psi_y}{\partial y}\right),\\&M_{xy}=\upsilon_1 D\left(\frac{\partial\psi_x}{\partial y}+\frac{\partial\psi_y}{\partial x}\right),\end{aligned} \tag{13}$$

$$\begin{aligned}&Q_{xz}=k\upsilon_1 A\left(\psi_x+\frac{\partial w}{\partial x}\right),\\&Q_{yz}=k\upsilon_1 A\left(\psi_y+\frac{\partial w}{\partial y}\right),\end{aligned}$$

in which $\upsilon_1=(1-\upsilon)/2$ and shear and bending rigidities are defined as

$$A=\int_{-\frac{h}{2}}^{\frac{h}{2}}\frac{E}{1-\upsilon^2}dz,\quad D=\int_{-\frac{h}{2}}^{\frac{h}{2}}\frac{Ez^2}{1-\upsilon^2}dz, \tag{14}$$

Also, external boundary conditions can be stated as follows [2]:

$$\begin{aligned}&M_{nn}=0\quad or\quad \psi_n=0,\\&M_{ns}=0\quad or\quad \psi_s=0,\\&Q_n=0\quad or\quad w=0,\end{aligned} \tag{15}$$

where normal and tangential components of bending moment and normal shear forced are defined as [2]

$$\begin{aligned}&M_{nn}=M_{xx}n_x^2+M_{yy}n_y^2+2M_{xy}n_x n_y,\\&M_{ns}=(M_{yy}-M_{xx})n_x n_y+M_{xy}(n_x^2-n_y^2),\\&Q_n=Q_{xz}n_x+Q_{yz}n_y,\\&n_x=\cos\theta,\\&n_y=\sin\theta.\end{aligned} \tag{16}$$

For the clamped edge (y=0), boundary conditions can be stated as [2]

$$w=0,\quad \psi_x=0,\quad \psi_y=0, \tag{17}$$

and for the free ones, following boundary conditions should be considered [2]:

$$M_{nn}=0,\quad M_{ns}=0,\quad Q_n=0. \tag{18}$$

For flutter analysis, the external force per unit area is created by the aerodynamic load and is expressed by the supersonic piston theory as [6]

$$f=\Delta p=-\xi\frac{\partial w}{\partial x}-\mu\frac{\partial w}{\partial t}, \tag{19}$$

in which ξ and μ are the aerodynamic pressure and damping parameters, respectively; these parameters are presented as

$$\xi=\frac{\rho_\infty U_\infty^2}{\sqrt{M_\infty^2-1}},\quad \mu=\frac{\rho_\infty U_\infty\left(M_\infty^2-2\right)}{\sqrt{\left(M_\infty^2-1\right)^3}}, \tag{20}$$

where M_∞ is Mach number.

As the aerodynamic damping term in Eq. (19) always stabilizes the flutter boundaries [24], to study the aeroelastic characteristics of the supersonic plate, the aerodynamic load without the aerodynamic damping is used to derive the flutter equation of the supersonic plate. Thus, inserting Eqs. (13) and (19) into the Eqs. (11), (16) and (18), the set of governing equations can be stated as

$$
\begin{aligned}
&k\upsilon_1 A\left(\frac{\partial\psi_x}{\partial x}+\frac{\partial\psi_y}{\partial y}+\frac{\partial^2 w}{\partial x^2}+\frac{\partial^2 w}{\partial y^2}\right)\\
&-\xi\frac{\partial w}{\partial x}-I_0\frac{\partial^2 w}{\partial t^2}=0,\\
&D\left(\frac{\partial^2\psi_x}{\partial x^2}+\upsilon_1\frac{\partial^2\psi_x}{\partial y^2}+\upsilon_2\frac{\partial^2\psi_y}{\partial x\,\partial y}\right)\\
&-k\upsilon_1 A\left(\psi_x+\frac{\partial w}{\partial x}\right)-I_2\frac{\partial^2\psi_x}{\partial t^2}=0,\\
&D\left(\upsilon_2\frac{\partial^2\psi_x}{\partial x\,\partial y}+\upsilon_1\frac{\partial^2\psi_y}{\partial x^2}+\frac{\partial^2\psi_y}{\partial y^2}\right)\\
&-k\upsilon_1 A\left(\psi_y+\frac{\partial w}{\partial y}\right)-I_2\frac{\partial^2\psi_y}{\partial t^2}=0,
\end{aligned}
\tag{21}
$$

and boundary conditions at the free edges can be written as

$$
\begin{aligned}
&\upsilon_3\frac{\partial\psi_x}{\partial x}+\upsilon_4\frac{\partial\psi_y}{\partial y}+2\upsilon_1\left(\frac{\partial\psi_x}{\partial y}+\frac{\partial\psi_y}{\partial x}\right)n_x n_y=0,\\
&2\left(-\frac{\partial\psi_x}{\partial x}+\frac{\partial\psi_y}{\partial y}\right)n_x n_y\\
&+\left(\frac{\partial\psi_x}{\partial y}+\frac{\partial\psi_y}{\partial x}\right)\left(n_x^2-n_y^2\right)=0,\\
&\left(\psi_x+\frac{\partial w}{\partial x}\right)n_x+\left(\psi_y+\frac{\partial w}{\partial y}\right)n_y=0,
\end{aligned}
\tag{22}
$$

in which

$$
\upsilon_2=0.5(1+\upsilon),\quad \upsilon_3=n_x^2+\upsilon n_y^2,\quad \upsilon_4=n_y^2+\upsilon n_x^2. \tag{23}
$$

Using Eqs. (2), (3), (12) and (14), following relations can be presented:

$$
\begin{aligned}
&A=A_c f_0,\qquad D=D_c f_2,\\
&I_0=\rho_c h g_0,\quad I_2=\frac{\rho_c h^3}{12}g_2,
\end{aligned}
\tag{24}
$$

where

$$
\begin{aligned}
A_c&=\frac{E_c h}{1-\upsilon^2},\quad D_c=\frac{E_c h^3}{12\left(1-\upsilon^2\right)},\\
f_0&=1+\left(\mu_E-1\right)\left(\kappa+\frac{1-\kappa}{q+1}\right),\\
g_0&=1+\left(\mu_\rho-1\right)\left(\kappa+\frac{1-\kappa}{q+1}\right),\\
f_2&=1+\left(\mu_E-1\right)\Theta(\kappa,q),\quad \mu_E=\frac{E_m}{E_c},\\
g_2&=1+\left(\mu_\rho-1\right)\Theta(\kappa,q),\quad \mu_\rho=\frac{\rho_m}{\rho_c},\\
\Theta(\kappa,q)&=\kappa^3+\frac{3(1-\kappa)\left[\kappa^2(q+1)(q+2)+2\kappa(q+1)+2\right]}{(q+1)(q+2)(q+3)}.
\end{aligned}
\tag{25}
$$

As Fig. 3 shows, the physical domain can be mapped into the computational domain using following transformation [2]:

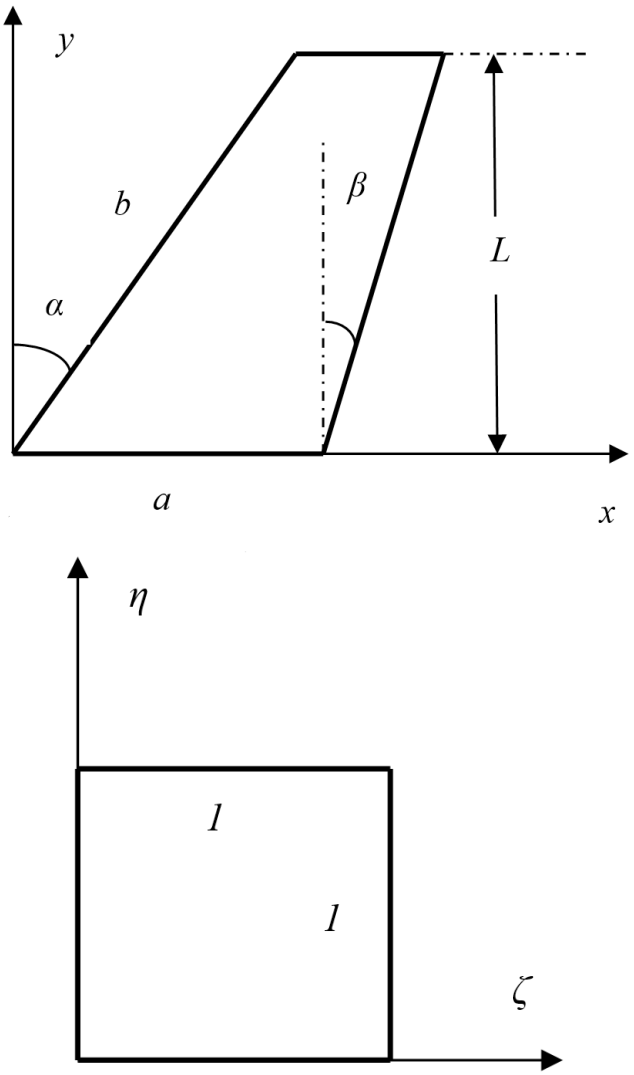

Fig. 3. Physical and computational domains [2].

$$
\begin{aligned}
x&=a\zeta+L\eta\left(\tan\alpha-G\zeta\right),\quad y=L\eta,\\
G&=\tan\alpha-\tan\beta.
\end{aligned}
\tag{26}
$$

Inverse form of Eq. (26) can be written as

$$
\zeta=\frac{x-y\tan\alpha}{a-Gy},\quad \eta=\frac{y}{L}, \tag{27}
$$

which leads to the following relations for derivatives:

$$
\begin{aligned}
&\frac{\partial}{\partial x}=\frac{H}{L}\frac{\partial}{\partial\zeta},\quad \frac{\partial^2}{\partial x^2}=\frac{H^2}{L^2}\frac{\partial^2}{\partial\zeta^2},\\
&\frac{\partial}{\partial y}=\frac{1}{L}\left(FH\frac{\partial}{\partial\zeta}+\frac{\partial}{\partial\eta}\right),\\
&\frac{\partial^2}{\partial y^2}=\frac{1}{L^2}\left(\begin{aligned}&F^2H^2\frac{\partial^2}{\partial\zeta^2}+2FH\frac{\partial^2}{\partial\zeta\partial\eta}\\&+\frac{\partial^2}{\partial\eta^2}+2GFH^2\frac{\partial}{\partial\zeta}\end{aligned}\right),\\
&\frac{\partial^2}{\partial x\,\partial y}=\frac{1}{L^2}\left(FH^2\frac{\partial^2}{\partial\zeta^2}+H\frac{\partial^2}{\partial\zeta\partial\eta}+GH^2\frac{\partial}{\partial\zeta}\right),
\end{aligned}
\tag{28}
$$

where

$$H=\frac{1}{\varphi\sec\alpha-G\eta},\quad F=G\zeta-\tan\alpha,\quad \varphi=\frac{a}{b}. \tag{29}$$

Considering ω as the eigen value and using the method of separation of variables as

$$\begin{Bmatrix} w(\zeta,\eta,t)\\ \psi_x(\zeta,\eta,t)\\ \psi_y(\zeta,\eta,t)\end{Bmatrix}=\begin{Bmatrix} bW(\zeta,\eta)\\ \Psi(\zeta,\eta)\\ \Phi(\zeta,\eta)\end{Bmatrix}e^{\omega t}, \tag{30}$$

the set of governing equations (21) can be rewritten as

$$\begin{aligned}
&k\upsilon_1\sec\alpha f_0\begin{bmatrix}(1+F^2)H^2W_{\zeta\zeta}+2FHW_{\zeta\eta}\\ +W_{\eta\eta}+2GFH^2W_{\zeta}\end{bmatrix}\\
&+k\upsilon_1 f_0\left(H\Psi_{\zeta}+FH\Phi_{\zeta}+\Phi_{\eta}\right)\\
&-\frac{\gamma^2\xi^*}{12\varphi^3}HW_{\zeta}=\lambda^2\frac{g_0\gamma^2\cos\alpha}{12}W,\\
&-\frac{12k\upsilon_1 f_0\cos\alpha}{\gamma^2}HW_{\zeta}+f_2H^2\left(1+\upsilon_1F^2\right)\Psi_{\zeta\zeta}\\
&+f_2\upsilon_1\left(2FH\Psi_{\zeta\eta}+\Psi_{\eta\eta}+2GFH^2\Psi_{\zeta}\right)\\
&-\frac{12k\upsilon_1 f_0\cos^2\alpha}{\gamma^2}\Psi\\
&+f_2\upsilon_2\left(FH^2\Phi_{\zeta\zeta}+H\Phi_{\zeta\eta}+GH^2\Phi_{\zeta}\right)\\
&=\lambda^2\frac{g_2\gamma^2\cos^2\alpha}{12}\Psi,\\
&-\frac{12k\upsilon_1 f_0\cos\alpha}{\gamma^2}\left(FHW_{\zeta}+W_{\eta}\right)\\
&+f_2\upsilon_2\left(FH^2\Psi_{\zeta\zeta}+H\Psi_{\zeta\eta}+GH^2\Psi_{\zeta}\right)\\
&+f_2\begin{bmatrix}(\upsilon_1+F^2)H^2\Phi_{\zeta\zeta}\\ +2FH\Phi_{\zeta\eta}+\Phi_{\eta\eta}+2GFH^2\Phi_{\zeta}\end{bmatrix}\\
&-\frac{12k\upsilon_1 f_0\cos^2\alpha}{\gamma^2}\Phi=\lambda^2\frac{g_2\gamma^2\cos^2\alpha}{12}\Phi,
\end{aligned} \tag{31}$$

where following dimensionless parameters are defined:

$$\gamma=\frac{h}{b},\quad \lambda^2=\frac{\rho_c h b^4\omega^2}{D_c},\quad \xi^*=\frac{\rho_\infty U_s^2a^3}{D_c}\frac{M_\infty^2}{\sqrt{M_\infty^2-1}}, \tag{32}$$

in which U_s is the velocity of sound. Also, dimensionless form of boundary conditions at the free edges can be stated as

$$\begin{aligned}
&\left(\upsilon_3+2\upsilon_1Fn_xn_y\right)H\Psi_{\zeta}+2\upsilon_1n_xn_y\Psi_{\eta}\\
&+\left(\upsilon_4F+2\upsilon_1n_xn_y\right)H\Phi_{\zeta}+\upsilon_4\Phi_{\eta}=0,\\
&\left[F\left(n_x^2-n_y^2\right)-2n_xn_y\right]H\Psi_{\zeta}+\left(n_x^2-n_y^2\right)\Psi_{\eta}\\
&+\left[n_x^2-n_y^2+2Fn_xn_y\right]H\Phi_{\zeta}+2n_xn_y\Phi_{\eta}=0,\\
&n_x\Psi+n_y\Phi+\sec\alpha\left[\left(n_x+Fn_y\right)HW_{\zeta}+W_{\eta}n_y\right]=0,
\end{aligned} \tag{33}$$

and at the clamped edge one can write:

$$\Psi=0,\quad \Phi=0,\quad W=0. \tag{34}$$

It should be noted that λ and ξ^* appeared in Eq. (32) are non-dimensional eigen value and non-dimensional aerodynamic pressure, respectively. These definitions are used by many authors and also are used here in this paper to validate the obtained results. Unfortunately, these definitions are not suitable to investigate the effects of dimensionless thickness or aspect ratio; because they contain a, b and h, simultaneously. Thus, in these cases following dimensionless definitions will be used:

$$\Lambda^2=\frac{12\left(1-\upsilon^2\right)\rho_c b^2\omega^2}{E_c},\quad \Gamma=\frac{\rho_\infty U_s^2}{E_c}\frac{M_\infty^2}{\sqrt{M_\infty^2-1}}, \tag{35}$$

which can be related to those in Eq. (32) as $\Lambda=\gamma\lambda$ and $\Gamma=\gamma^3\xi^*/[12(1-\nu^2)\varphi^3]$.

3- Differential Quadrature Method

The values of function $f(\zeta,\eta)$ at $N\times M$ pre-selected grid of points can be considered as

$$f_{ij}=f\left(\zeta_i,\eta_j\right)\quad \begin{matrix} i=1,2,...,N\\ j=1,2,...,M\end{matrix}. \tag{36}$$

According to the differential quadrature rules, all derivatives of the function can be approximated by means of weighted linear sum of the function values at the pre-selected grid of points as

$$\begin{aligned}
&\left.\frac{\partial f}{\partial\zeta}\right|_{(\zeta,\eta)=(\zeta_i,\eta_j)}=\sum_{n=1}^{N}A_{in}^{(\zeta)}f_{nj},\\
&\left.\frac{\partial^2 f}{\partial\zeta^2}\right|_{(\zeta,\eta)=(\zeta_i,\eta_j)}=\sum_{n=1}^{N}B_{in}^{(\zeta)}f_{nj},\\
&\left.\frac{\partial f}{\partial\eta}\right|_{(\zeta,\eta)=(\zeta_i,\eta_j)}=\sum_{m=1}^{M}A_{jm}^{(\eta)}f_{im},\\
&\left.\frac{\partial^2 f}{\partial\eta^2}\right|_{(\zeta,\eta)=(\zeta_i,\eta_j)}=\sum_{m=1}^{M}B_{jm}^{(\eta)}f_{im},\\
&\left.\frac{\partial^2 f}{\partial\zeta\partial\eta}\right|_{(\zeta,\Theta)=(\zeta_i,\eta_j)}=\sum_{n=1}^{N}A_{in}^{(\zeta)}\sum_{m=1}^{M}A_{jm}^{(\eta)}f_{nm},
\end{aligned} \tag{37}$$

where $A(\zeta)$, $B(\zeta)$, $A(\eta)$ and $B(\eta)$ are the weighting coefficients associated with the first and second order derivatives in ζ and η directions, respectively. These matrices for the first-order derivatives are given as [25]

$$A_{in}^{(\zeta)}=\begin{cases}\dfrac{\prod_{\substack{k=1\\k\neq i,n}}^{N}(\zeta_i-\zeta_k)}{\prod_{\substack{k=1\\k\neq n}}^{N}(\zeta_n-\zeta_k)}, & (i,n=1,2,3,...,N;i\neq n)\\ \sum_{\substack{k=1\\k\neq i}}^{N}\dfrac{1}{(\zeta_i-\zeta_k)}, & (i=n=1,2,3,...,N)\end{cases} \tag{38}$$

$$A_{jm}^{(\eta)} = \begin{cases} \dfrac{\prod_{\substack{k=1 \\ k\neq j,m}}^{M}(\eta_j-\eta_k)}{\prod_{\substack{k=1 \\ k\neq m}}^{M}(\eta_m-\eta_k)}, & (j,m=1,2,3,...,M;\ j\neq m) \\ \sum_{\substack{k=1 \\ k\neq j}}^{M}\dfrac{1}{(\eta_j-\eta_k)}, & (j=m=1,2,3,...,M) \end{cases}$$

and of second-order derivatives are extracted from the following relations:

$$B^{(\zeta)} = A^{(\zeta)}A^{(\zeta)}, \quad B^{(\eta)} = A^{(\eta)}A^{(\eta)}. \tag{39}$$

Eq. (37) can be written in the following matrix form:

$$\begin{aligned} &\left[f_\zeta\right]=\left[A^{(\zeta)}\right][f], \quad \left[f_{\zeta\zeta}\right]=\left[B^{(\zeta)}\right][f], \\ &\left[f_\eta\right]=[f]\left[A^{(\eta)}\right]^T, \quad \left[f_{\eta\eta}\right]=[f]\left[B^{(\eta)}\right]^T, \\ &\left[f_{\zeta\eta}\right]=\left[A^{(\zeta)}\right][f]\left[B^{(\eta)}\right]^T, \end{aligned} \tag{40}$$

in which superscript T indicates transpose operator.
For a matrix $[f]_{N\times M}$, an equivalent column vector $\{\bar{f}\}_{NM\times 1}$ can be defined as [2]

$$\bar{f}_v = f_{ij}, \quad v=(j-1)N+i. \tag{41}$$

Using this technique, a multiple of three matrices as $[a][f][b]$ can be replaced by $([b]^T\otimes[a])\{\bar{f}\}$; in which $\otimes$ indicates the Kronecker product [2]. Therefore, Eq. (40) can be written as

$$\begin{aligned} &\left\{\bar{f}_\zeta\right\}=\left(I^\eta\otimes\left[A^{(\zeta)}\right]\right)\left\{\bar{f}\right\}, \\ &\left\{\bar{f}_{\zeta\zeta}\right\}=\left(I^\eta\otimes\left[B^{(\zeta)}\right]\right)\left\{\bar{f}\right\}, \\ &\left\{\bar{f}_\eta\right\}=\left(\left[A^{(\eta)}\right]\otimes I^\zeta\right)\left\{\bar{f}\right\}, \\ &\left\{\bar{f}_{\eta\eta}\right\}=\left(\left[B^{(\eta)}\right]\otimes I^\zeta\right)\left\{\bar{f}\right\}, \\ &\left\{\bar{f}_{\zeta\eta}\right\}=\left(\left[A^{(\eta)}\right]\otimes\left[A^{(\zeta)}\right]\right)\left\{\bar{f}\right\}, \end{aligned} \tag{42}$$

where I^ζ and I^η indicate the identity matrix of size N and M, respectively.
In addition to the number of grid points, distribution of them affects the convergence of the solution. A well-accepted set of the grid points is the Gauss–Lobatto–Chebyshev points given for interval [0,1] as

$$\begin{aligned} &\zeta_i=\frac{1}{2}\left\{1-\cos\left[\frac{(i-1)\pi}{(N-1)}\right]\right\}, \quad i=1,2,...,N. \\ &\eta_j=\frac{1}{2}\left\{1-\cos\left[\frac{(j-1)\pi}{M-1}\right]\right\}, \quad j=1,2,...,M. \end{aligned} \tag{43}$$

4- DQ Analogue

Using DQ rules, the set of governing differential equations (31) is transformed to the following form:

$$[K]\{u\}=\lambda^2[M]\{u\}, \tag{44}$$

where [K] and [M] are stiffness and mass matrices which are presented in detail in Appendix A. Also, in a similar manner boundary conditions (33) and (34) can be written using DQ rules as

$$[T]\{u\}=\{0\}, \tag{45}$$

in which components of the matrix [T] are presented in Appendix B.
In two dimensional problems, three kinds of points can be considered: interior points, boundary points, and corner points. As each corner point belongs to two adjacent edges, in this paper the relations of both corresponding edges are considered for each corner point. Implementation of conditions at corner points is a very well-known issue in DQM and the wrong implementation leads to numerical instabilities of the solution. Interested readers can find more details in Refs. [26-34].
Let us divide the grid points as two sets: boundary points which are located at the four edges of the plate and domain ones which are other internal points. By neglecting satisfying the Eq. (44) at the boundary points, this equation can be written as [35]

$$\left[\bar{K}\right]\{u\}=\lambda^2\left[\bar{M}\right]\{u\}, \tag{46}$$

where bar sign implies the corresponding non-square matrix. Eqs. (45) and (46) may be rearranged and partitioned in order to separate the boundary (b) and domain (d) points as follows:

$$\begin{aligned} &\left[\bar{K}\right]_d\{u\}_d+\left[\bar{K}\right]_b\{u\}_b= \\ &\lambda^2\left(\left[\bar{M}\right]_d\{u\}_d+\left[\bar{M}\right]_b\{u\}_b\right), \end{aligned} \tag{47a}$$

$$[T]_d\{u\}_d+[T]_b\{u\}_b=\{0\}. \tag{47b}$$

Inserting Eq. (47-b) into Eq. (47-a) leads to the following eigen value equation:

$$[F_K]\{u\}_d=\lambda^2[F_M]\{u\}_d, \tag{48}$$

in which

$$\begin{aligned} &[F_K]=\left[\bar{K}\right]_d-\left[\bar{K}\right]_b[T]_b^{-1}[T]_d, \\ &[F_M]=\left[\bar{M}\right]_d-\left[\bar{M}\right]_b[T]_b^{-1}[T]_d. \end{aligned} \tag{49}$$

Using Eq. (48) the eigen values and corresponding modes can be obtained. It should be noted that obtained eigen values are the complex numbers. Thus, non-dimensional frequency (Ω or χ) and corresponding dimensionless damping ratio (ζ^*) are defined as [36]:

$$\Omega=\mathrm{Im}(\lambda), \quad \chi=\mathrm{Im}(\Lambda), \quad \zeta^*=-\frac{\mathrm{Re}(\lambda)}{|\lambda|}=-\frac{\mathrm{Re}(\Lambda)}{|\Lambda|}. \tag{50}$$

in which Re(λ), Im(λ) and $|\lambda|$ indicate real part, imaginary part and the absolute value of complex number λ, respectively.

Table 2. Convergence of the presented solution.

Number of grid points (N=M)	Mode number					
	1	2	3	4	5	6
5	4.994123	15.73193	25.54740	66.21993	70.35063	141.7747
6	5.582063	21.20373	21.20373	45.20371	57.70620	64.73268
7	5.607089	12.20261	23.79906	37.76262	59.66677	66.75532
8	5.539882	24.70848	24.70848	59.66378	61.05909	67.76939
9	5.548298	13.20464	23.98945	39.77785	60.75835	67.44721
10	5.513786	13.46191	24.06631	39.89909	60.48502	67.41541
11	5.523723	13.25988	24.03058	40.04180	60.40756	67.18627
12	5.509811	13.29344	24.02721	39.87433	60.41811	67.29120
13	5.516232	13.22507	24.01777	39.91001	60.39515	67.22431
14	5.509912	13.23108	24.01283	39.83484	60.39309	67.23351
15	5.513123	13.20868	24.01093	39.84369	60.38694	67.20047
16	5.510241	13.21109	24.00899	39.81622	60.38494	67.21137
17	5.511544	13.20322	24.00892	39.81825	60.38341	67.20259
18	5.510285	13.20533	24.00824	39.80923	60.38285	67.20302

5- Numerical results and discussion

In this section, numerical results are presented for the developed solution in the previous sections. First, the convergence of the presented solution should be examined. For this purpose, consider a functionally graded sandwich plate of κ=1/3, q=2, α=20°, β=10°, φ=0.75 and γ=0.05 imposed on a supersonic compressible flow of ξ^*=10. The effect of the number of grid points (N=M) on the value of the first six frequencies is presented in Table 2. As shown in this table, 15 grid points at each direction are adequate for the convergence of the first six frequencies and this number of points will be used for all of the following examples.

In order to check the accuracy of the proposed numerical solution, a homogenous trapezoidal plate of E=68.2 GPa, υ=0.35, ρ=2860 kg/m^3, a=8.8 cm, b=10.35 cm, h=0.98 mm, α=27° and β=-13° is considered. Table 3 shows the value of the first six frequencies and corresponding experimental ones reported by Romero et al. [37]. Except for the fifth mode which has a considerable difference, Table 3 shows an excellent agreement between the presented numerical solution and experimental tests. For more assurance, corresponding modes are depicted and are compared with experimental ones in Figs. 4(a-f). These figures confirm high accuracy of the presented solution.

In order to check the effect of aerodynamic pressure and also validate the proposed solution for the flutter analysis, two cases of a homogeneous plate of φ=1 and γ=0.01 are considered. For a rectangular plate, Figs. 5(a-b) show the variation of first two dimensionless frequencies and corresponding damping ratios versus variation of non-dimensional aerodynamic pressure. As these figures show the increase in aerodynamic pressure leads to an increase in the first frequency and a decrease in the second one. At ξ^*=61.25, these two frequencies become equal to Ω=6.69 and the corresponding value of damping ratio of the second mode drops to the negative values. In fact, at this point, the aeroelastic self-excited oscillation of the plate occurs which is known as the aeroelastic flutter. The value of the aerodynamic pressure at this point is called critical aerodynamic pressure and the corresponding frequency is called the flutter frequency.

Similar diagrams are depicted in Figs. 6(a-b) for a skew plate (α=β=30°). As shown in these figures, the non-dimensional critical aerodynamic pressure is ξ^*=37.5 and non-dimensional flutter frequency is Ω=8.56. It is clearly seen from Figs. 5(a) to 6(b) that the flutter characteristics obtained by calculating the natural frequencies are the same as those obtained by calculating the damping ratios. It should be noted that it cannot be concluded if the aerodynamic damping term in Eq. (19) be considered.

In Table 4, non-dimensional critical aerodynamic pressure and non-dimensional flutter frequencies are listed and are compared with those presented by other authors based on FEM. This comparison confirms the high accuracy of the presented solution. It is worth mentioning that in comparison with GDQM, the most advantage of FEM is its strength in solve problems with complicated geometries. But, for problems with simple geometries which can be solved by both methods, GDQM has less computational efforts.

The convergence and versatility of the proposed solution were confirmed in previous examples. Thus, the effect of various parameters on the flutter boundaries can be investigated. In order to investigate the effect of power law index on flutter

Table 3. Comparison of the presented solution with experimental results [37].

Mode number	Natural frequency (Hz)					
	1	2	3	4	5	6
Presented	153.1031	579.5874	676.4468	1492.844	1735.459	2291.54
Experimental [37]	153	594	717	1571	1970	2320
Difference (%)	0.067353	-2.42637	-5.65595	-4.97491	-11.9056	-1.22671

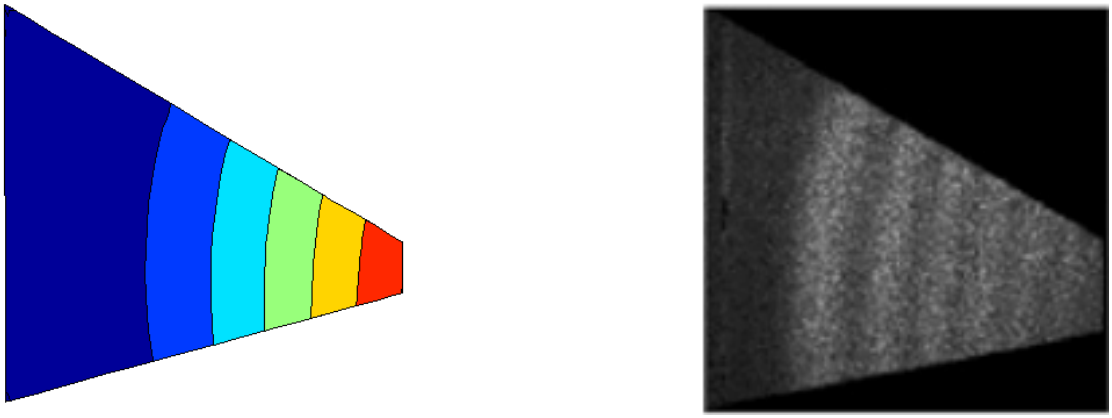

(a) Mode 1

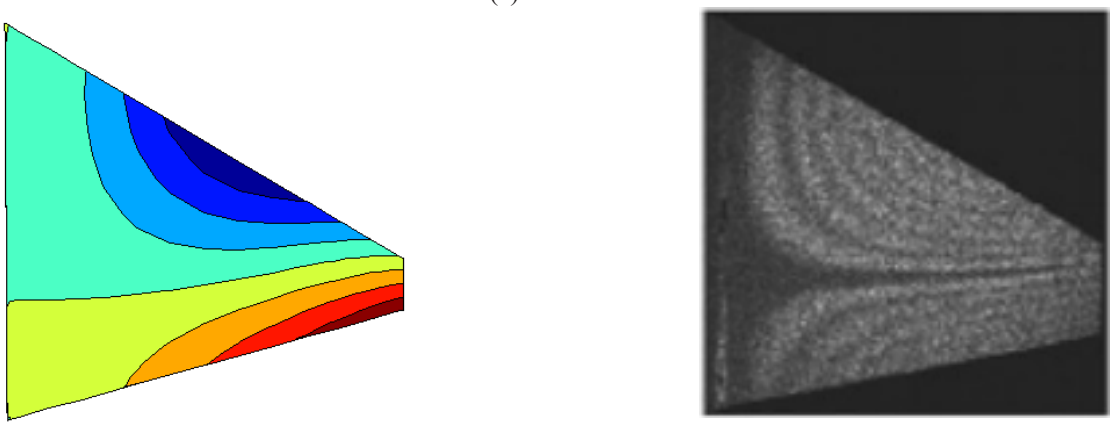

(b) Mode 2

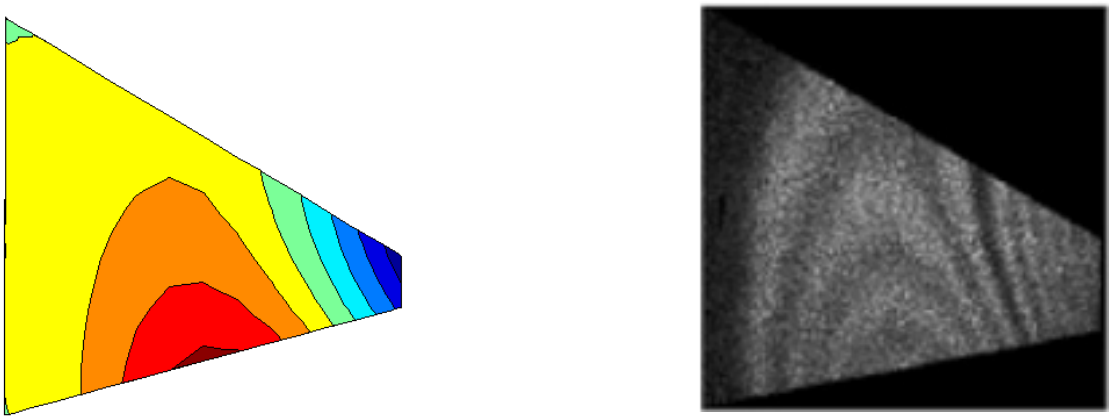

(c) Mode 3

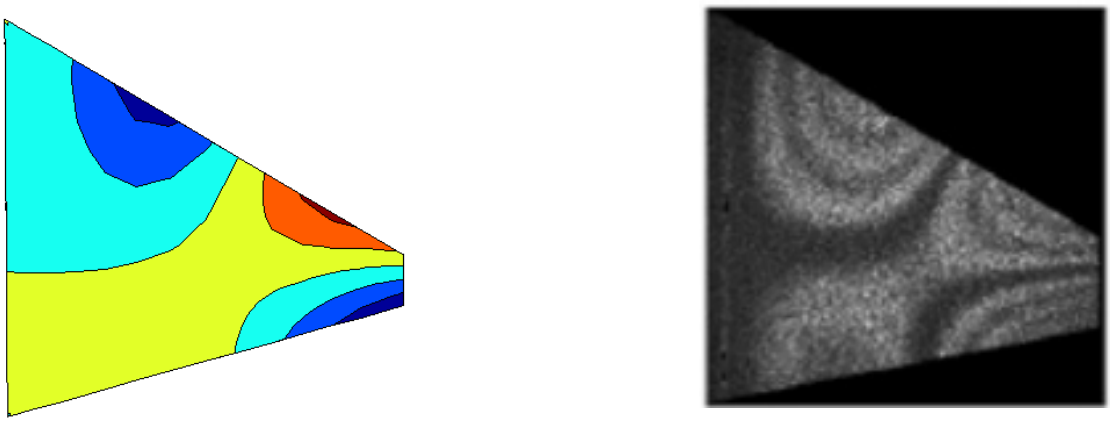

(d) Mode 4

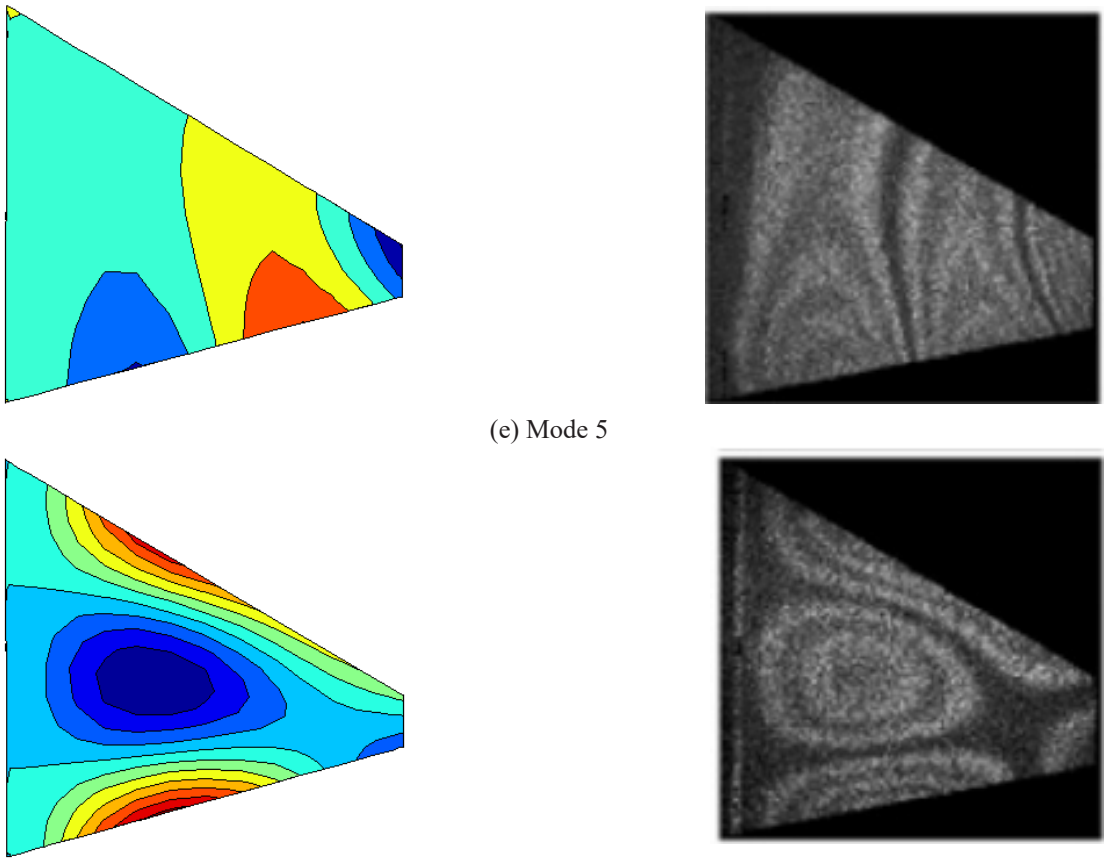

(e) Mode 5

(f) Mode 6

Fig. 4. Comparison between presented modes and experimental results [37].

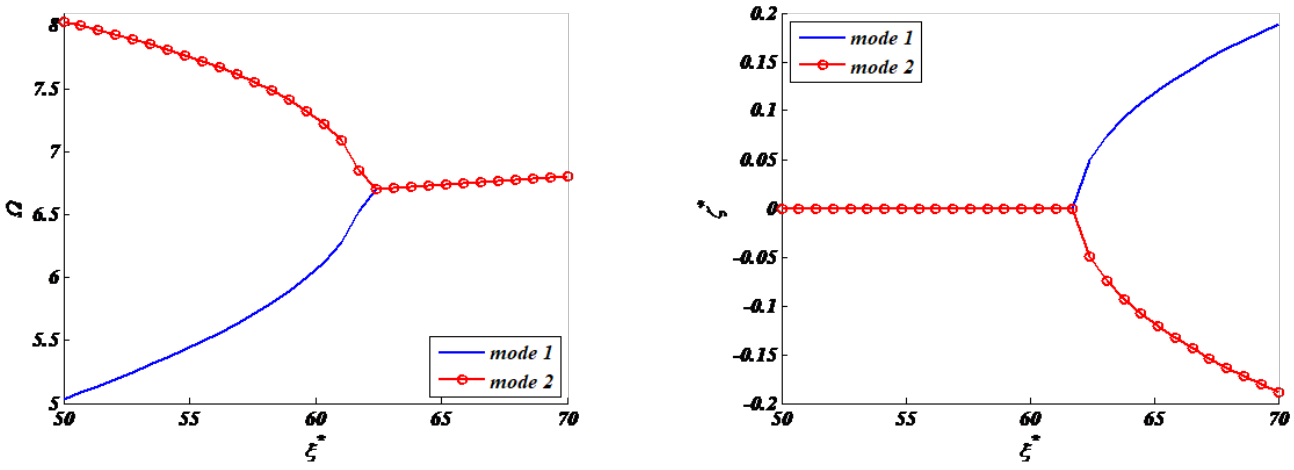

(a) (b)

Fig. 5. Variation of the first two dimensionless frequencies (a) and corresponding damping ratios (b) of a rectangular plate versus variation of non-dimensional aerodynamic pressure.

Table 4. Non-dimensional critical aerodynamic pressure and non-dimensional flutter frequencies for rectangular and skew plates.

$\alpha=\beta$	ξ^*_{cr}			Ω_{cr}		
	present	FEM		present	FEM	
		Chowdary et al. [4]	Singha and Ganapathi [5]		Chowdary et al. [4]	Singha and Ganapathi [5]
0	61.25	59.51	57.89	6.69	6.48	-
30°	37.5	41.12	40.04	8.56	8.13	-

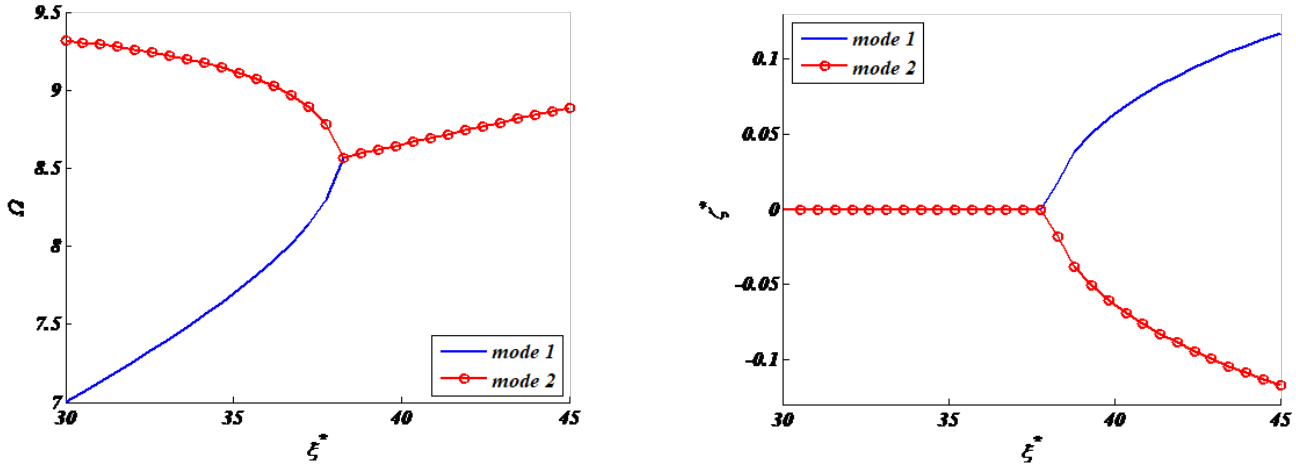

(a) (b)

Fig. 6. Variation of the first two dimensionless frequencies (a) and corresponding damping ratios (b) of a skew plate versus variation of non-dimensional aerodynamic pressure.

boundaries consider a functionally graded sandwich plate of κ=0.25, α=25°, β=-5°, φ=0.75 and γ=0.01. In Figs. 7(a-d) the variation of the first six dimensionless frequencies versus non-dimensional aerodynamic pressure is depicted for various values of power-law index. As these figures show, an increase in the value of q increases both critical aerodynamic pressure and flutter frequency. It is worth mentioning that as Fig. 2 shows, the increment in the value of the q increases the volume fraction of the ceramic which increases both stiffness and mass of the plate.

A functionally graded sandwich plate of q=1, α=20°, β=5°, φ=0.5 and γ=0.01 is considered for the study variation of flutter boundaries of functionally graded sandwich plates by the variation of the thickness of the core (κ). Variation of the first six dimensionless frequencies versus non-dimensional aerodynamic pressure is depicted in Figs. 8(a-d) for the various values of κ. These figures show that increment in the value of κ decreases both critical aerodynamic pressure and flutter frequency. It should be noticed that as Fig. 2 shows, increase in the value of the κ decreases both stiffness and mass of the plate.

Figs. 7 and 8 show that increment in the value of volume fraction of the ceramic (increase in q or decrease in κ), makes plate more stable. However, Table 1 shows that density of Al_2O_3 is higher than Al and these attempts make the plate heavier which is not the desired item in aircrafts.

The effect of material properties on the flutter boundaries was investigated in Figs. 7 and 8 and in what follows, the effects of geometrical parameters on the flutter boundaries of functionally graded sandwich plates are investigated.

Angles of leading and trailing edges of wing and fin tail have a significant effect on dynamic and aerodynamic characteristics of aircrafts. In order to investigate the effect of angles of leading edge (α), consider a functionally graded sandwich plate of κ=0.2, q=3, β=10°, φ=0.5 and γ=0.02. For the various values of α, a variation of the first six dimensionless frequencies is illustrated versus non-dimensional aerodynamic pressure in Figs. 9(a-d). These figures indicate that as the value of α increases, a rise can be seen in the values of the non-dimensional critical aerodynamic pressure and makes the plate more stable.

In practice, unlike the angle of leading edge (α) the value of the angle of trailing edge (β) can be either positive or negative. In order to investigate the effect of this parameter, a functionally graded sandwich plate of κ=0.5, q=0.25, α=30°, φ=0.8 and γ=0.015 is considered.

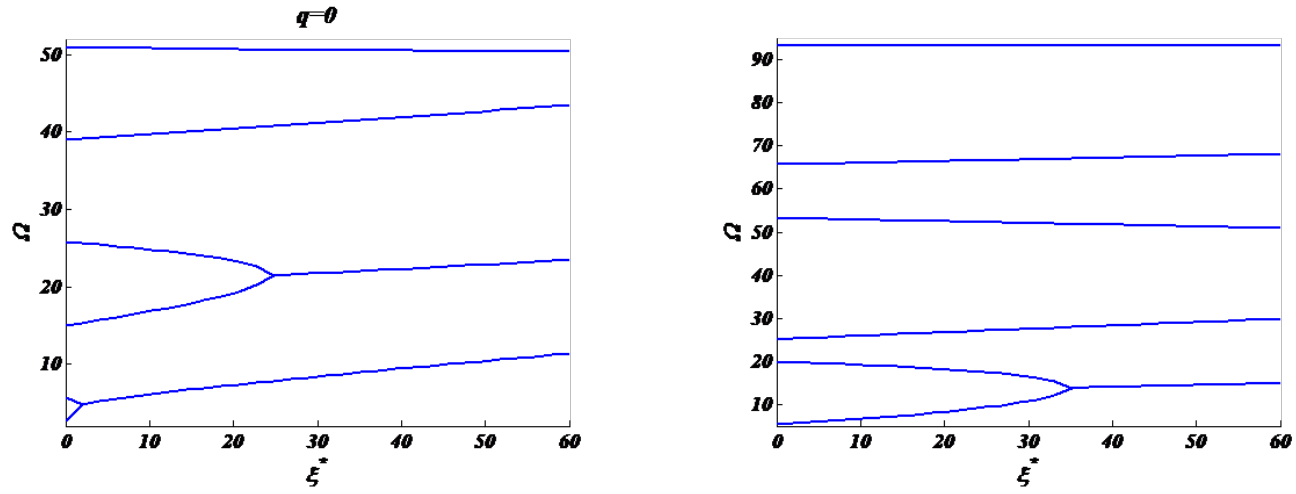

(a) q=0 (b) q=0.5

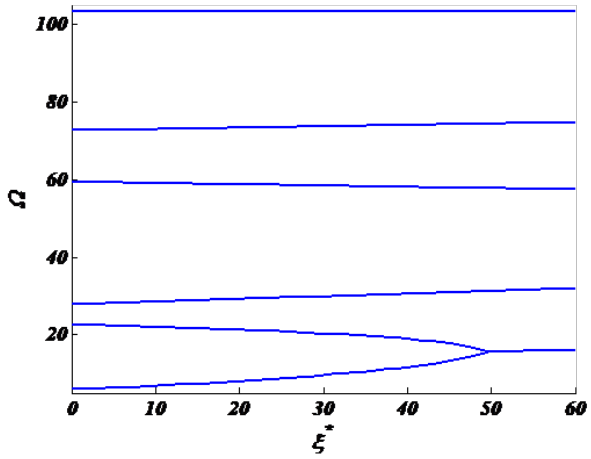

(c) q=1

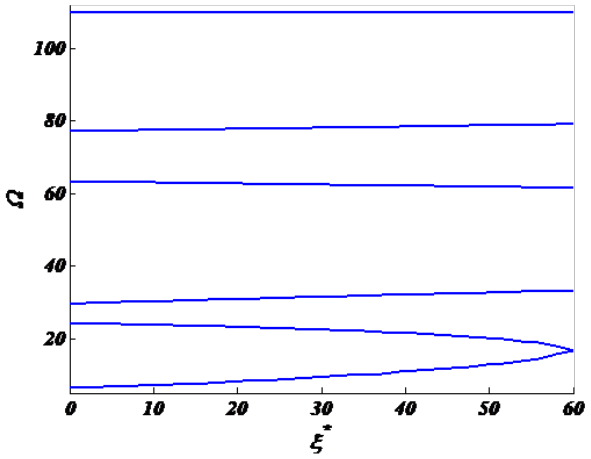

(d) q=2

Fig. 7. Variation of the first six dimensionless frequencies for a functionally graded sandwich plate versus variation of non-dimensional aerodynamic pressure for various values of power-law index.

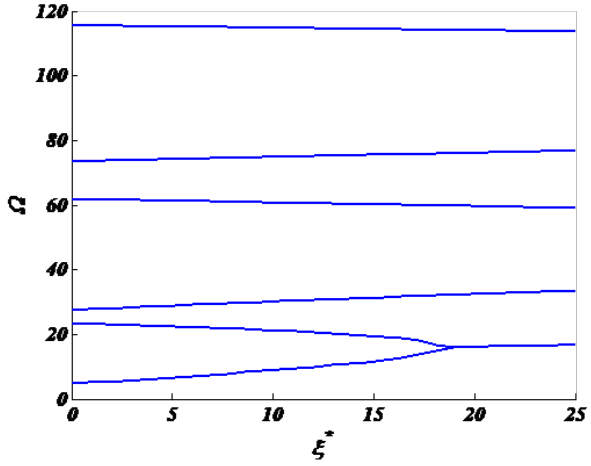

(a) κ=0

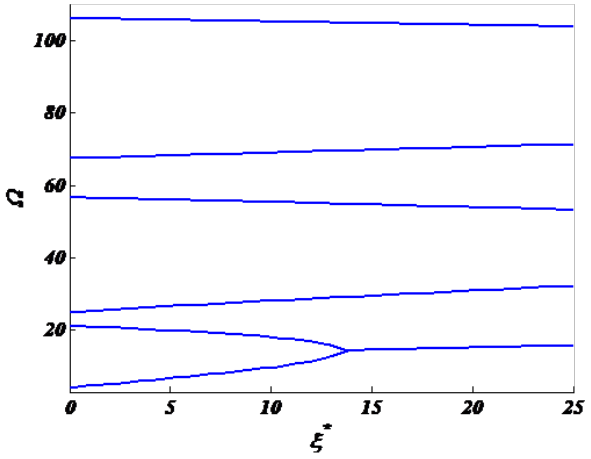

(b) κ=0.5

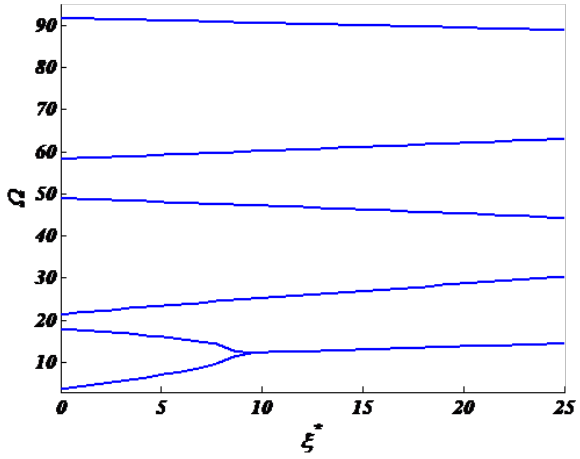

(c) κ=0.75

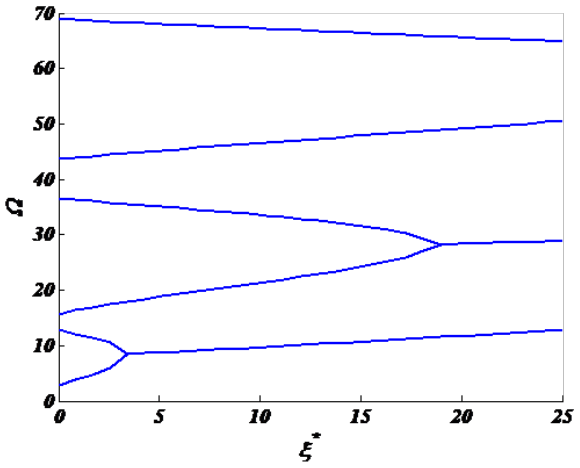

(d) κ=0.95

Fig. 8. Variation of the first six dimensionless frequencies for a functionally graded sandwich plate versus variation of non-dimensional aerodynamic pressure for various values of κ.

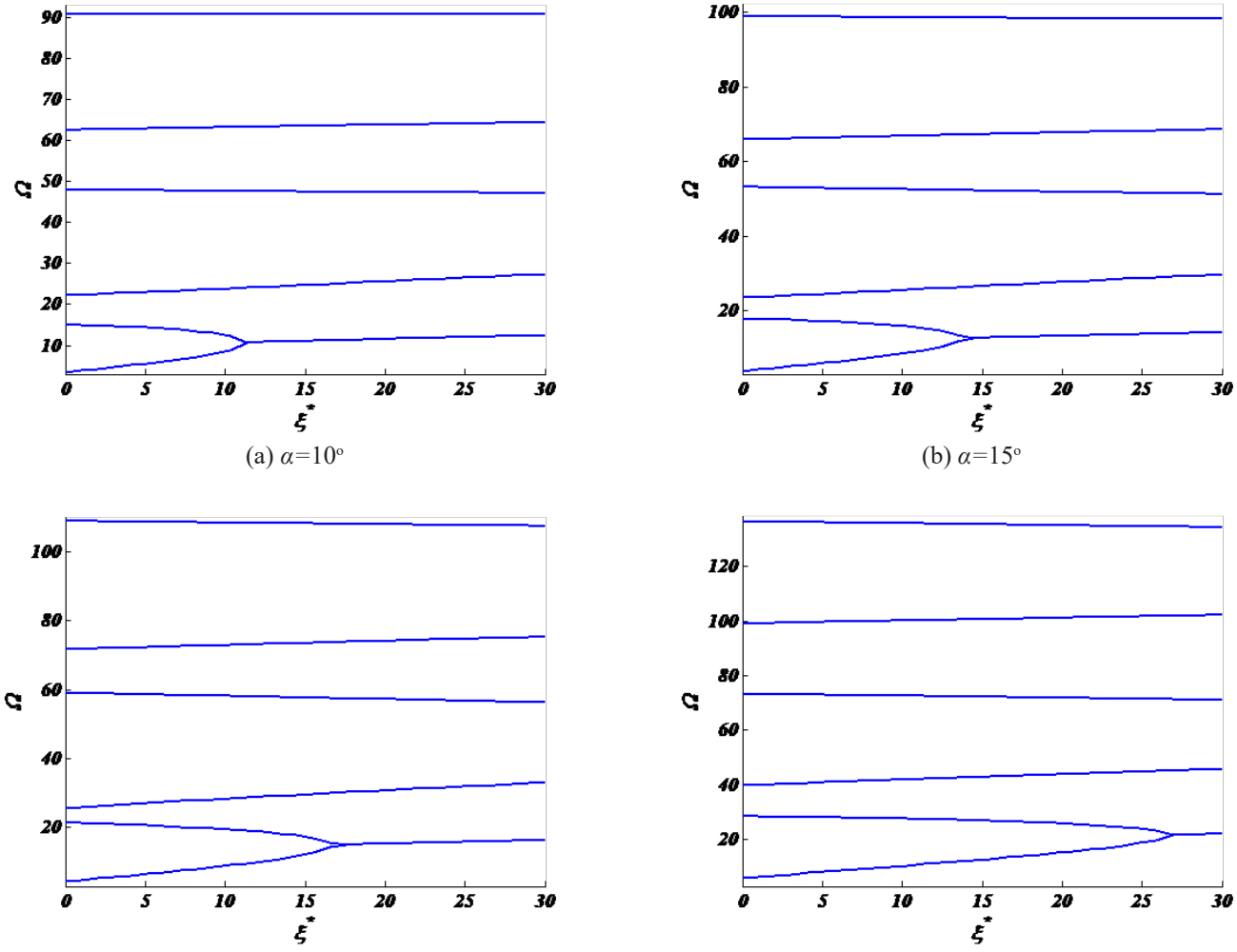

(a) α=10° (b) α=15°

(c) α=20° (d) α=30°

Fig. 9. Variation of the first six dimensionless frequencies for a functionally graded plate versus variation of non-dimensional aerodynamic pressure for various values of angles of leading edge (α).

Figs. 10(a-g) show a variation of first six dimensionless frequencies versus non-dimensional aerodynamic pressure for various values of β. These figures show that critical aerodynamic pressure and flutter frequency of the plates with negative values of β are greater than those with positive values of β. It can be seen that as the value of the angle of trailing edge changes from negative values to positive ones, critical aerodynamic pressure decrease and the plate becomes more unstable.

It is expected that aerodynamic characteristics of the plate to be affected by its thickness and aspect ratio. As said, in order to investigate the effect of non-dimensional thickness and aspect ratio on the flutter boundaries, it is better to use the dimensionless forms of aerodynamic pressure and frequency presented in Eq. (35). Consider a functionally graded sandwich plate of κ=0.2, q=7, α=15°, β=-5° and φ=0.4. For various values of dimensionless thickness, Figs. 11(a-d) show a variation of first six dimensionless frequencies versus non-dimensional aerodynamic pressure. As these figures show, the increment in the thickness of the plate increases critical aerodynamic pressure. In other words, an increase in thickness makes plate more stable; but it makes the plate heavier, as well.

A functionally graded sandwich plate of κ=0.3, q=4, α=30°, β=10°, γ=0.01 is considered to study the effect of aspect ratio on flutter boundaries. In Figs. 12(a-d) a variation of the first six dimensionless frequencies versus non-dimensional aerodynamic pressure is illustrated for various values of the

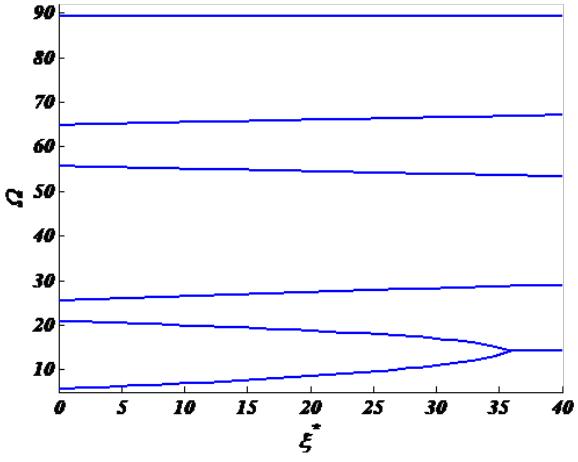

(a) β=-15°

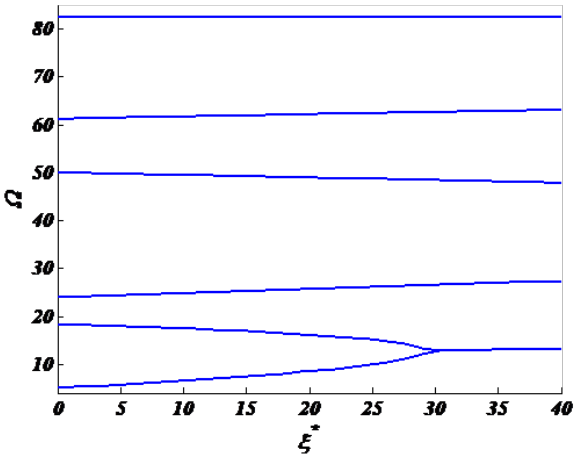

(b) β=-10°

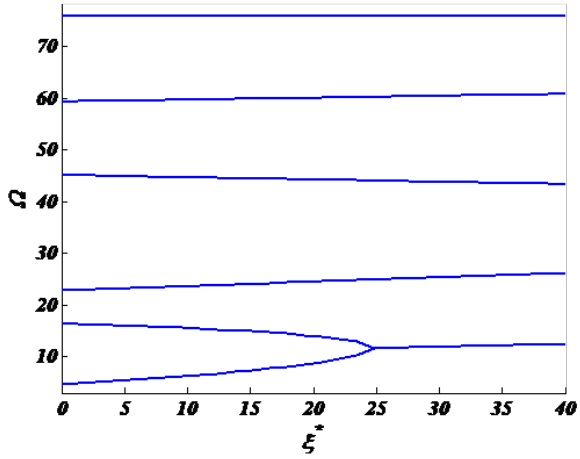

(c) β=-5°

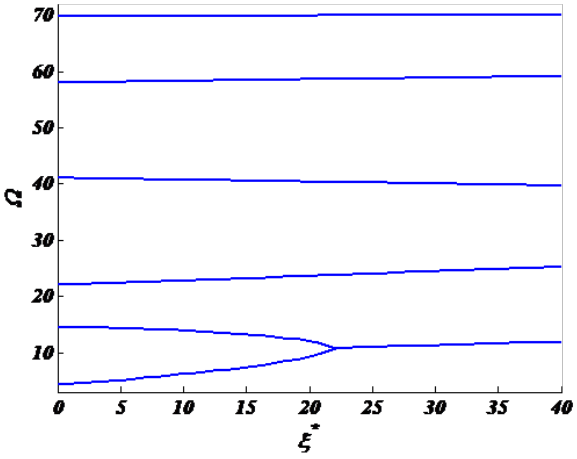

(d) β=0°

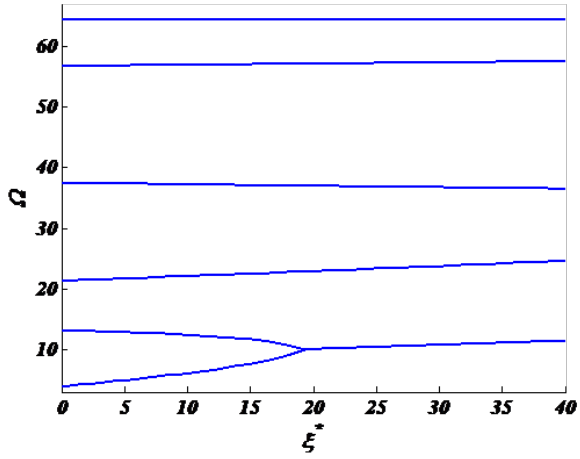

(e) β=5°

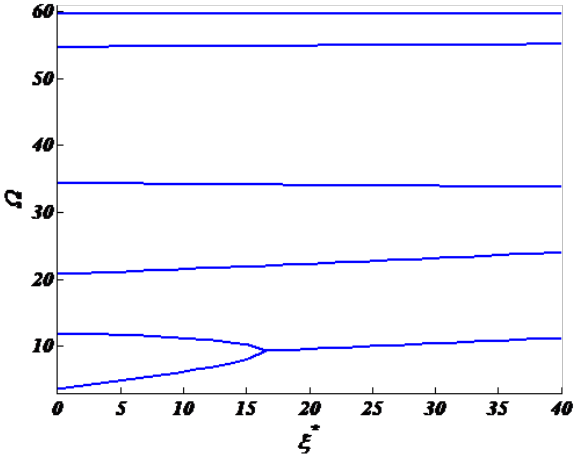

(f) β=10°

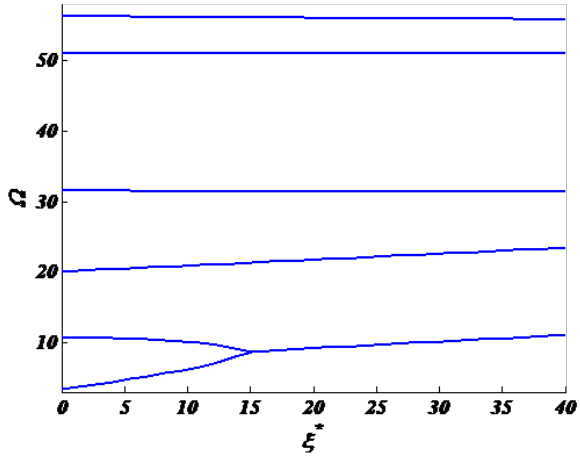

(g) β=15°

Fig. 10. Variation of the first six dimensionless frequencies for a functionally graded sandwich plate versus variation of non-dimensional aerodynamic pressure for various values of angles of trailing edge (β).

aspect ratio. As depicted in these figures, the increment in aspect ratio decreases both critical aerodynamic pressure. In other words, for plates with a bigger width, it is more likely for flutter to happen. It can be concluded that in order to increase the stability of the plate, it is better to decrease its width; but this attempt leads to the decreased area of the plate which reduces the total lift force of the aircraft.

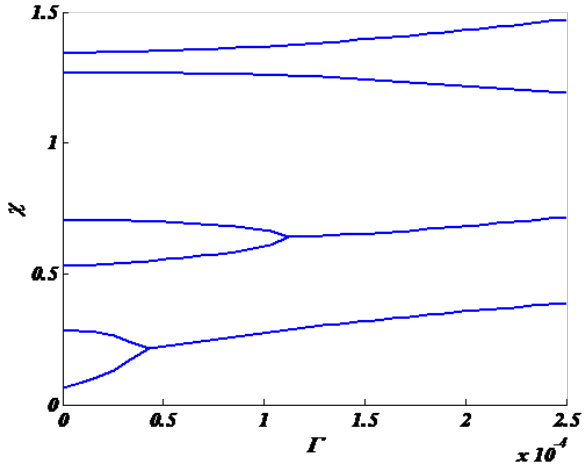

(a) γ=0.01

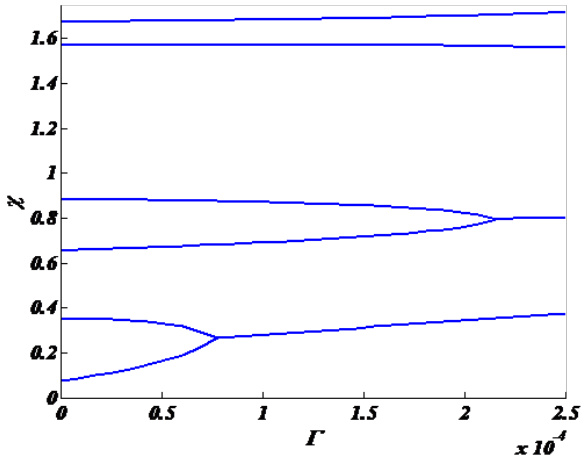

(b) γ=0.0125

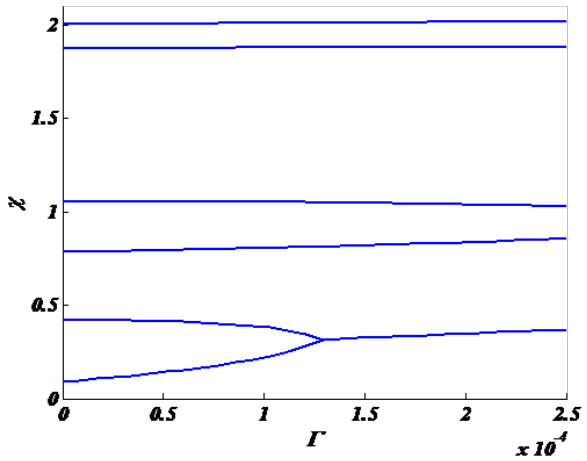

(c) γ=0.015

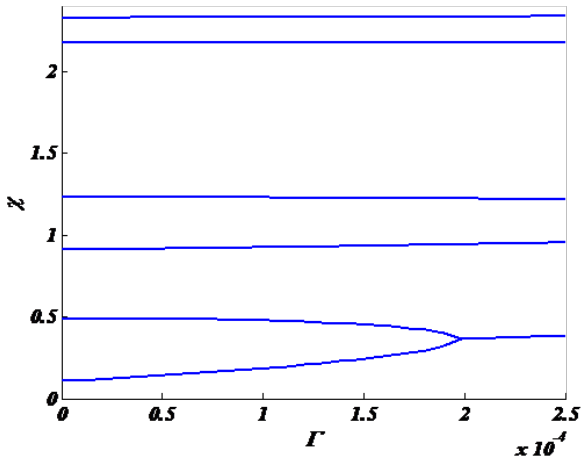

(d) γ=0.0175

Fig. 11. Variation of the first six dimensionless frequencies for a functionally graded sandwich plate versus variation of non-dimensional aerodynamic pressure for various values of dimensionless thickness.

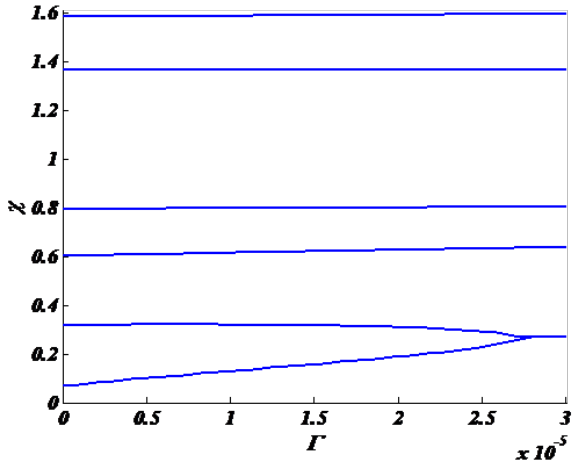

(a) φ=0.4

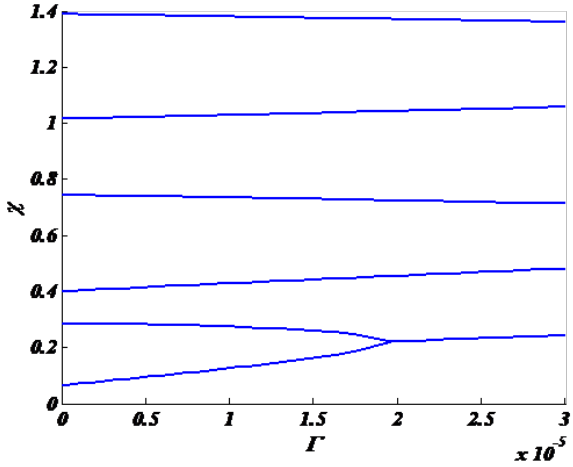

(b) φ=0.5

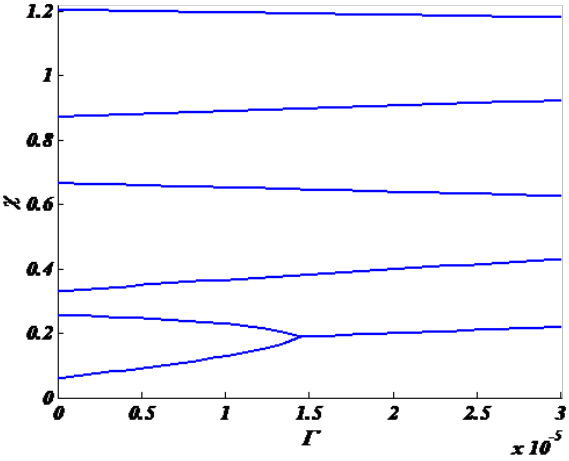

(c) φ=0.6

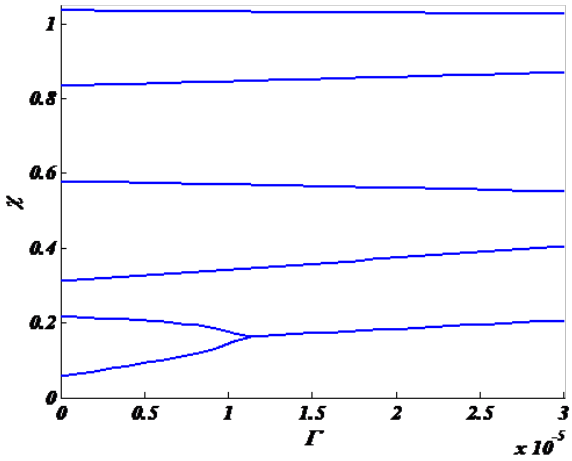

(d) φ=0.7

Fig. 12. Variation of the first six dimensionless frequencies for a functionally graded sandwich plate versus variation of non-dimensional aerodynamic pressure for various values of aspect ratio.

6- Conclusion

Using GDQM numerical solution was presented for the supersonic flutter analysis of cantilevered trapezoidal functionally graded sandwich plates. The first shear deformation plate theory and supersonic piston theory were used to model the structure and aerodynamic pressure, respectively. Numerical results revealed that in order to increase critical aerodynamic pressure and stability of the plate, the following attempts can be made:

1. Increasing the value of the angle of leading edge (α) as far as possible.
2. If possible, using negative values for the angle of leading edge (β) instead of positive ones.
3. Increasing angle of leading edge (β) if this angle is negative and decreasing this angle if this angle is positive.
4. Decreasing the width of the plate as far as possible. It is worth mentioning that all of the above-mentioned attempts lead to a decrease in the total area of the plate and therefore will decrease the lift force, which is not desired in aircrafts.
5. Increasing the thickness of the plate as far as possible.
6. Increase in volume fraction of a ceramic part of the plate as far as possible. It can be achieved by increasing power law index (q) or decreasing thickness of the core (κ).

It should be noticed that the two last attempts lead to a rise in the total weight of the plate which is not the desired item for aircrafts.

It seems that any attempt to increase the critical aerodynamic pressure of the plate leads to a decrease in the lift force or rise in the weight of the plate which is not desired for aircrafts. Thus, considering the maximum allowable value for the weight and minimum allowable value for lift force (area) as design constraints, optimum values of material variation parameters (κ and q) and geometrical parameters (α, β, γ and φ) can be found to increase the stability (critical aerodynamic pressure) of the plate. This constrained optimization is considered by authors as a topic for future studies.

Appendix A

Components of stiffness and mass matrices used in Eq. (44) are presented as

$$[K]=\begin{bmatrix} k_{WW} & k_{W\Psi} & k_{W\Phi} \\ k_{\Psi W} & k_{\Psi\Psi} & k_{\Psi\Phi} \\ k_{\Phi W} & k_{\Phi\Psi} & k_{\Phi\Phi} \end{bmatrix},$$
$$[M]=\begin{bmatrix} m_W & [0] & [0] \\ [0] & m_\Psi & [0] \\ [0] & [0] & m_\Phi \end{bmatrix}, \tag{A1}$$

where [0] indicates null matrix of size MN*MN and following matrices are defined:

$$k_{WW}=k\upsilon_1 f_0 \sec\alpha \begin{pmatrix} [b]^2\otimes\left\{\left(I^\zeta+[a]^2\right)\left[B^\zeta\right]\right\} \\ +2\left([b]\left[A^\eta\right]\right)\otimes\left([a]\left[A^\zeta\right]\right) \\ +\left[B^\eta\right]\otimes I^\zeta+2G[b]^2\otimes\left([a]\left[A^\zeta\right]\right) \end{pmatrix}$$
$$-\frac{\gamma^2\xi^*}{12\varphi^3}[b]\otimes\left[A^\zeta\right]$$
$$k_{W\Psi}=k\upsilon_1 f_0[b]\otimes\left[A^\zeta\right]$$
$$k_{W\Phi}=k\upsilon_1 f_0\left\{[b]\otimes\left([a]\left[A^\zeta\right]\right)+\left[A^\eta\right]\otimes I^\zeta\right\},$$
$$k_{\Psi W}=-\frac{12k\upsilon_1 f_0\cos\alpha}{\gamma^2}[b]\otimes\left[A^\zeta\right], \tag{A2}$$
$$k_{\Psi\Psi}=f_2[b]^2\otimes\left\{\left(I^\zeta+\upsilon_1[a]^2\right)\left[B^\zeta\right]\right\}$$
$$-\frac{12k\upsilon_1 f_0\cos^2\alpha}{\gamma^2}I^\eta\otimes I^\zeta$$
$$+f_2\upsilon_1\begin{Bmatrix} 2\left([b]\left[A^\eta\right]\right)\otimes\left([a]\left[A^\zeta\right]\right) \\ +\left[B^\eta\right]\otimes I^\zeta+2G[b]^2\otimes\left([a]\left[A^\zeta\right]\right) \end{Bmatrix},$$
$$k_{\Psi\Phi}=f_2\upsilon_2\begin{Bmatrix} [b]^2\otimes\left([a]\left[B^\zeta\right]\right) \\ +\left([b]\left[A^\eta\right]\right)\otimes\left[A^\zeta\right]+G[b]^2\otimes\left[A^\zeta\right] \end{Bmatrix},$$

$$k_{\Phi W} = -\frac{12k\upsilon_1 f_0 \cos\alpha}{\gamma^2}\left\{[b]\otimes\left([a]\left[A^{\zeta}\right]\right)+\left[A^{\eta}\right]\otimes I^{\zeta}\right\},$$

$$k_{\Phi\Psi} = f_2\upsilon_2\begin{Bmatrix}[b]^2\otimes\left([a]\left[B^{\zeta}\right]\right)\\ +\left([b]\left[A^{\eta}\right]\right)\otimes\left[A^{\zeta}\right]+G[b]^2\otimes\left[A^{\zeta}\right]\end{Bmatrix},$$

$$k_{\Phi\Phi} = f_2\begin{Bmatrix}[b]^2\otimes\left\{\left(\upsilon_1 I^{\zeta}+[a]^2\right)\left[B^{\zeta}\right]\right\}\\ +2\left([b]\left[A^{\eta}\right]\right)\otimes\left([a]\left[A^{\zeta}\right]\right)+\left[B^{\eta}\right]\otimes I^{\zeta}\\ +2G[b]^2\otimes\left([a]\left[A^{\zeta}\right]\right)\end{Bmatrix}$$

$$-\frac{12k\upsilon_1 f_0\cos^2\alpha}{\gamma^2}I^{\eta}\otimes I^{\zeta},$$

$$m_W = \cos\alpha\frac{g_0\gamma^2}{12}I^{\eta}\otimes I^{\zeta},$$

$$m_{\Psi} = m_{\Phi} = \cos^2\alpha\frac{g_2\gamma^2}{12}I^{\eta}\otimes I^{\zeta},$$

and following diagonal matrices are considered:

$$a_{ii} = F\left(\zeta_i\right),\quad b_{jj} = H\left(\eta_j\right),\quad \begin{matrix}i=1,2,3,\ldots,N\\ j=1,2,3,\ldots,M\end{matrix}. \tag{A1}$$

Appendix B

Definition of the matrix [T] appeared in Eq. (45) are presented as follows:

$$[T] = \begin{bmatrix}T_{11} & T_{12} & T_{13}\\ T_{21} & T_{22} & T_{23}\\ T_{31} & T_{32} & T_{33}\\ T_{41} & T_{42} & T_{43}\\ T_{51} & T_{52} & T_{53}\\ T_{61} & T_{62} & T_{63}\\ T_{71} & T_{72} & T_{73}\\ T_{81} & T_{82} & T_{83}\\ T_{91} & T_{92} & T_{93}\\ T_{101} & T_{102} & T_{103}\\ T_{111} & T_{112} & T_{113}\\ T_{121} & T_{121} & T_{123}\end{bmatrix}, \tag{B1}$$

where components of this matrix are related to the boundary conditions at four edges of the plate as:
at edge η=0:

$$\begin{aligned}&T_{11} = T_{22} = T_{33} = I_{1j}^{\eta}\otimes I^{\zeta},\\ &T_{12} = T_{13} = T_{21} = T_{23} = T_{31} = T_{32} = \{0\}_{N*NM}.\end{aligned} \tag{B2}$$

at edge η=1:

$$\begin{aligned}&T_{41} = T_{51} = T_{62} = \{0\}_{N*NM},\\ &T_{42} = \upsilon H(1)\left(I_{Mj}^{\eta}\otimes A^{\zeta}\right),\\ &T_{43} = T_{52} = \frac{T_{61}}{\sec\alpha} = H(1)\left(I_{Mj}^{\eta}\otimes[a]\left[A^{\zeta}\right]\right)+A_{Mj}^{\eta}\otimes I^{\zeta},\\ &T_{53} = H(1)\left(I_{Mj}^{\eta}\otimes\left[A^{\zeta}\right]\right),\\ &T_{63} = I_{Mj}^{\eta}\otimes I^{\zeta},\end{aligned} \tag{B3}$$

at edge ζ=0:

$$\begin{aligned}&T_{71} = T_{81} = \{0\}_{M*NM},\\ &T_{72} = \left[\upsilon_3+2\upsilon_1 F(0)n_x n_y\right]\left([b]\otimes A_{1i}^{\zeta}\right)\\ &+2\upsilon_1 n_x n_y\left(\left[A^{\eta}\right]\otimes I_{1i}^{\zeta}\right),\\ &T_{73} = \left[\upsilon_4 F(0)+2\upsilon_1 n_x n_y\right]\left([b]\otimes A_{1i}^{\zeta}\right)+\upsilon_4\left(\left[A^{\eta}\right]\otimes I_{1i}^{\zeta}\right),\\ &T_{82} = \left[F(0)\left(n_x^2-n_y^2\right)-2n_x n_y\right]\left([b]\otimes A_{1i}^{\zeta}\right)\\ &+\left(n_x^2-n_y^2\right)\left(\left[A^{\eta}\right]\otimes I_{1i}^{\zeta}\right),\\ &T_{83} = \left[n_x^2-n_y^2+2F(0)n_x n_y\right]\left([b]\otimes A_{1i}^{\zeta}\right)\\ &+2n_x n_y\left(\left[A^{\eta}\right]\otimes I_{1i}^{\zeta}\right),\\ &T_{91} = \sec\alpha\begin{Bmatrix}\left[n_x+F(0)n_y\right]\left([b]\otimes A_{1i}^{\zeta}\right)\\ +n_y\left(\left[A^{\eta}\right]\otimes I_{1i}^{\zeta}\right)\end{Bmatrix},\\ &T_{92} = n_x\left(I^{\eta}\otimes I_{1i}^{\zeta}\right),\\ &T_{93} = n_y\left(I^{\eta}\otimes I_{1i}^{\zeta}\right),\end{aligned} \tag{B4}$$

where

$$n_x = -\cos\alpha,\quad n_y = \sin\alpha. \tag{B5}$$

and finally at edge ζ=1:

$$\begin{aligned}&T_{101} = T_{111} = \{0\}_{M*NM},\\ &T_{102} = \left[\upsilon_3+2\upsilon_1 F(1)n_x n_y\right]\left([b]\otimes A_{Ni}^{\zeta}\right)\\ &+2\upsilon_1 n_x n_y\left(\left[A^{\eta}\right]\otimes I_{Ni}^{\zeta}\right),\\ &T_{103} = \left[\upsilon_4 F(1)+2\upsilon_1 n_x n_y\right]\left([b]\otimes A_{Ni}^{\zeta}\right)\\ &+\upsilon_4\left(\left[A^{\eta}\right]\otimes I_{Ni}^{\zeta}\right),\\ &T_{112} = \left[F(1)\left(n_x^2-n_y^2\right)-2n_x n_y\right]\left([b]\otimes A_{Ni}^{\zeta}\right)\\ &+\left(n_x^2-n_y^2\right)\left(\left[A^{\eta}\right]\otimes I_{Ni}^{\zeta}\right),\\ &T_{113} = \left[n_x^2-n_y^2+2F(1)n_x n_y\right]\left([b]\otimes A_{Ni}^{\zeta}\right)\\ &+2n_x n_y\left(\left[A^{\eta}\right]\otimes I_{Ni}^{\zeta}\right),\\ &T_{121} = \sec\alpha\begin{Bmatrix}\left[n_x+F(1)n_y\right]\left([b]\otimes A_{Ni}^{\zeta}\right)\\ +n_y\left(\left[A^{\eta}\right]\otimes I_{Ni}^{\zeta}\right)\end{Bmatrix},\\ &T_{122} = n_x\left(I^{\eta}\otimes I_{Ni}^{\zeta}\right),\\ &T_{123} = n_y\left(I^{\eta}\otimes I_{Ni}^{\zeta}\right),\end{aligned} \tag{B6}$$

in which

$$n_x = \cos\beta,\quad n_y = -\sin\beta. \tag{B7}$$

It should be noted that in Eqs. (B2) - (B6), the following obvious relations are considered:

$$\begin{aligned}&H(1) = \frac{1}{\varphi\sec\alpha-G},\\ &F(0) = -\tan\alpha,\quad F(1) = -\tan\beta.\end{aligned} \tag{B7}$$

References

[1] K. Torabi, H. Afshari, Generalized differential quadrature method for vibration analysis of cantilever trapezoidal FG thick plate, *Journal of Solid Mechanics*, 8(1) (2016) 184-203.

[2] K. Torabi, H. Afshari, Vibration analysis of a cantilevered trapezoidal moderately thick plate with variable thickness, *Engineering Solid Mechanics*, 5(1) (2017) 71-92.

[3] R. Srinivasan, B. Babu, Flutter analysis of cantilevered quadrilateral plates, *Journal of Sound and Vibration*, 98(1) (1985) 45-53.

[4] T. Chowdary, P. Sinha, S. Parthan, Finite element flutter analysis of composite skew panels, *Computers & structures*, 58(3) (1996) 613-620.

[5] M.K. Singha, M. Ganapathi, A parametric study on supersonic flutter behavior of laminated composite skew flat panels, *Composite structures*, 69(1) (2005) 55-63.

[6] T. Prakash, M. Ganapathi, Supersonic flutter characteristics of functionally graded flat panels including thermal effects, *Composite Structures*, 72(1) (2006) 10-18.

[7] M. Singha, M. Mandal, Supersonic flutter characteristics of composite cylindrical panels, *Composite Structures*, 82(2) (2008) 295-301.

[8] S.-Y. Kuo, Flutter of rectangular composite plates with variable fiber pacing, *Composite Structures*, 93(10) (2011) 2533-2540.

[9] M.-C. Meijer, L. Dala, Zeroth-order flutter prediction for cantilevered plates in supersonic flow, *Journal of Fluids and Structures*, 57 (2015) 196-205.

[10] A. Sankar, S. Natarajan, T.B. Zineb, M. Ganapathi, Investigation of supersonic flutter of thick doubly curved sandwich panels with CNT reinforced facesheets using higher-order structural theory, *Composite Structures*, 127 (2015) 340-355.

[11] A. Cunha-Filho, A. de Lima, M. Donadon, L. Leão, Flutter suppression of plates using passive constrained viscoelastic layers, *Mechanical Systems and Signal Processing*, 79 (2016) 99-111.

[12] H. Navazi, H. Haddadpour, Nonlinear aero-thermoelastic analysis of homogeneous and functionally graded plates in supersonic airflow using coupled models, *Composite Structures*, 93(10) (2011) 2554-2565.

[13] V.V. Vedeneev, Panel flutter at low supersonic speeds, *Journal of fluids and structures*, 29 (2012) 79-96.

[14] V.V. Vedeneev, Effect of damping on flutter of simply supported and clamped panels at low supersonic speeds, *Journal of Fluids and Structures*, 40 (2013) 366-372.

[15] H. Haddadpour, S. Mahmoudkhani, H. Navazi, Supersonic flutter prediction of functionally graded cylindrical shells, *Composite Structures*, 83(4) (2008) 391-398.

[16] S. Mahmoudkhani, H. Haddadpour, H. Navazi, Supersonic flutter prediction of functionally graded conical shells, *Composite Structures*, 92(2) (2010) 377-386.

[17] M. Kouchakzadeh, M. Rasekh, H. Haddadpour, Panel flutter analysis of general laminated composite plates, *Composite Structures*, 92(12) (2010) 2906-2915.

[18] J. Li, Y. Narita, Analysis and optimal design for supersonic composite laminated plate, *Composite Structures*, 101 (2013) 35-46.

[19] J. Li, Y. Narita, Multi-objective design for aeroelastic flutter of laminated shallow shells under variable flow angles, *Composite Structures*, 111 (2014) 530-539.

[20] K. Torabi, H. Afshari, Optimization for flutter boundaries of cantilevered trapezoidal thick plates, *Journal of the Brazilian Society of Mechanical Sciences and Engineering*, 39(5) (2017) 1545-1561.

[21] S. Hosseini-Hashemi, M. Fadaee, S.R. Atashipour, A new exact analytical approach for free vibration of Reissner–Mindlin functionally graded rectangular plates, *International Journal of Mechanical Sciences*, 53(1) (2011) 11-22.

[22] R. Mindlin, Influence of rotatory inertia and shear on flexural motions of isotropic, elastic plates, *J. appl. Mech.*, 18 (1951) 31.

[23] T. Kaneko, On Timoshenko's correction for shear in vibrating beams, *Journal of Physics D: Applied Physics*, 8(16) (1975) 1927.

[24] W.-H. Shin, I.-K. Oh, J.-H. Han, I. Lee, Aeroelastic characteristics of cylindrical hybrid composite panels with viscoelastic damping treatments, *Journal of Sound and Vibration*, 296(1) (2006) 99-116.

[25] C.W. Bert, M. Malik, Differential quadrature method in computational mechanics: a review, *Applied Mechanics Reviews*, 49 (1996) 1-28.

[26] E. Viola, F. Tornabene, N. Fantuzzi, Generalized differential quadrature finite element method for cracked composite structures of arbitrary shape, *Composite Structures*, 106 (2013) 815-834.

[27] N. Fantuzzi, F. Tornabene, Strong formulation finite element method for arbitrarily shaped laminated plates–Part I. Theoretical analysis, *Adv. Aircr. Spacecr. Sci*, 1(2) (2014).

[28] N. Fantuzzi, F. Tornabene, Strong formulation finite element method for arbitrarily shaped laminated plates–Part II. Numerical analysis, *Adv. Aircr. Spacecr. Sci*, 1(2) (2014).

[29] N. Fantuzzi, F. Tornabene, E. Viola, A. Ferreira, A strong formulation finite element method (SFEM) based on RBF and GDQ techniques for the static and dynamic analyses of laminated plates of arbitrary shape, *Meccanica*, 49(10) (2014) 2503-2542.

[30] F. Tornabene, N. Fantuzzi, F. Ubertini, E. Viola, Strong formulation finite element method based on differential quadrature: a survey, *Applied Mechanics Reviews*, 67(2) (2015) 020801.

[31] N. Fantuzzi, F. Tornabene, E. Viola, Four-parameter functionally graded cracked plates of arbitrary shape: a GDQFEM solution for free vibrations, *Mechanics of Advanced Materials and Structures*, 23(1) (2016) 89-107.

[32] N. Fantuzzi, M. Bacciocchi, F. Tornabene, E. Viola, A.J. Ferreira, Radial basis functions based on differential quadrature method for the free vibration analysis

of laminated composite arbitrarily shaped plates, *Composites Part B: Engineering*, 78 (2015) 65-78.

[33] N. Fantuzzi, F. Tornabene, Strong Formulation Isogeometric Analysis (SFIGA) for laminated composite arbitrarily shaped plates, *Composites Part B: Engineering*, 96 (2016) 173-203.

[34] F. Tornabene, N. Fantuzzi, M. Bacciocchi, A.M. Neves, A.J. Ferreira, MLSDQ based on RBFs for the free vibrations of laminated composite doubly-curved shells, *Composites Part B: Engineering*, 99 (2016) 30-47.

[35] H. Du, M. Lim, R. Lin, Application of generalized differential quadrature method to structural problems, *International Journal for Numerical Methods in Engineering*, 37(11) (1994) 1881-1896.

[36] J. Gao, W. Liao, Vibration analysis of simply supported beams with enhanced self-sensing active constrained layer damping treatments, *Journal of Sound and Vibration*, 280(1) (2005) 329-357.

[37] G. Romero, L. Alvarez, E. Alaní, L. Nallim, R. Grossi, Study of a vibrating plate: comparison between experimental (ESPI) and analytical results, *Optics and lasers in engineering*, 40(1) (2003) 81-90.

Please cite this article using:

H. Afshari and K. Torabi, A Parametric Study on Flutter Analysis of Cantilevered Trapezoidal FG Sandwich Plates,

AUT J. Mech. Eng., 1(2) (2017) 191-210.

DOI: 10.22060/mej.2017.12329.5314